REPORT DOCUMENTATION PAGE	Form Approved OMB No. 0704-0188

PLEASE DO NOT RETURN YOUR FORM TO THE ABOVE ADDRESS.

1. REPORT DATE *(DD-MM-YYYY)*	2. REPORT TYPE	3. DATES COVERED *(From - To)*
3/1/2012	Final report (in advance of end of project)	7/15/09-3/1/2012

4. TITLE AND SUBTITLE

COMPACT FIBER-PARAMETRIC DEVICES FOR BIOPHOTONICS APPLICATIONS

5a. CONTRACT NUMBER

FA9550-09-1-0483

5b. GRANT NUMBER

5c. PROGRAM ELEMENT NUMBER

6. AUTHOR(S)

Jay E. Sharping

5d. PROJECT NUMBER

5e. TASK NUMBER

5f. WORK UNIT NUMBER

7. PERFORMING ORGANIZATION NAME(S) AND ADDRESS(ES)

University of California Merced
5200 N. Lake Road
Merced, CA 95343

8. PERFORMING ORGANIZATION REPORT NUMBER

9. SPONSORING/MONITORING AGENCY NAME(S) AND ADDRESS(ES)

AFOSR

10. SPONSOR/MONITOR'S ACRONYM(S)

11. SPONSOR/MONITOR'S REPORT NUMBER(S)

AFRL-OSR-VA-TR-2012-0681

12. DISTRIBUTION/AVAILABILITY STATEMENT

Distribution A: approved for public release

13. SUPPLEMENTARY NOTES

14. ABSTRACT

This project involved the simulation, development, testing, and application of several working fiber optical parametric oscillators. System simulation codes were developed in Matlab and used to predict and understand performance. Optical fiber and pulse characterization systems were assembled and used to study commercial microstructure fibers as well as noncommercial fibers provided by collaborators. Three versions of the light source were implemented: 1) a 100 femtosecond system operating near 1000 nm, 2) a picosecond system operating near 1000 nm, and 3) a picosecond system operating near 780 nm, A fourth "directly-modulated mostly-fiber" version operating near 1000 nm is under construction. The systems were applied in a coherent anti-Stokes Raman scattering microscopy experiment to chemically resolve cell features.

15. SUBJECT TERMS

16. SECURITY CLASSIFICATION OF:			17. LIMITATION OF ABSTRACT	18. NUMBER OF PAGES	19a. NAME OF RESPONSIBLE PERSON
a. REPORT	b. ABSTRACT	c. THIS PAGE		120	Jay E. Sharping
					19b. TELEPHONE NUMBER *(Include area code)* 209 217 7233

Final Report Date: 3/1/2012

To: technicalreports@afosr.af.mil

Subject: Final Statement to Howard Schlossberg

Contract/Grant Title: Compact fiber-parametric devices for biophotonics applications

Contract/Grant #: FA9550-09-1-0483 P00002

Reporting Period: 14-07-2010 – 1-3-2012

Archival publications (published) during reporting period:

1. C. Gu, C. Goulart, and J. E. Sharping, "Cross-phase-modulation-induced spectral effects in high-efficiency picosecond fiber optical parametric oscillators," Opt. Lett. **36,** 1488-1490 (2011).

2. C. Gu and J. Sharping,"XPM-Induced Spectral Distortion in High Efficiency, Picosecond, Fiber Optical Parametric Oscillators" OFC (Optical Society of America, 2011).

3. J. E. Sharping,"Analysis of ultrashort pulsed FOPOs" CLEO (Optical Society of America, 2011).

4. Y. H. Zhai, C. Goulart, J. E. Sharping, H. F. Wei, S. Chen, W. J. Tong, M. N. Slipchenko, D. Zhang, and J. X. Cheng, "Multimodal coherent anti-Stokes Raman spectroscopic imaging with a fiber optical parametric oscillator," Appl. Phys. Lett. **98,** (2011).

5. C. J. Gu, H. F. Wei, S. Chen, W. J. Tong, and J. E. Sharping, "Fiber optical parametric oscillator for sub-50 fs pulse generation: optimization of fiber length," Opt. Lett. **35,** 3516-3518 (2010).

6. C. Gu, J. Sharping, H. Wei, and W. Tong,"Fiber Length Optimization in a Dispersion Compensated Fiber Optical Parametric Oscillator" in *Conference on Lasers and Electro-Optics* (Optical Society of America, 2010).

7. J. E. Sharping, W. Q. Zhang, and S. A. V.,"Modeling of Ultrafast Fiber Optical Parametric Oscillators" in *Frontiers in Optics*(Optical Society of America, 2010).

8. Y. Zhai, C. Pailo, M. Slipchenko, D. Zhang, H. Wei, S. Chen, W. Tong, J. Cheng, and J. E. Sharping,"Fiber OPO for Multimodal CARS Imaging" in *Frontiers in Optics* (Optical Society of America, 2010).

9. W. Q. Zhang, J. E. Sharping, R. T. White, T. M. Monro, and V. S. Afshar, "Design and optimization of fiber optical parametric oscillators for femtosecond pulse generation," Optics Express 18, 17294-17305 (2010).

10. C. Gu, J. Sharping, H. Wei, and W. Tong, "Chirped Sub-50 fs Pulse Generation: Optimization of Fiber Length for Ultrafast Fiber Optical Parametric Oscillators," in *Optical Fiber Communication Conference,* Anonymous (Optical Society of America, 2010), pp. OTuJ4.

11. C. Gu, J. Sharping, H. Wei, and W. Tong, "Fiber Length Optimization in a Dispersion Compensated Fiber Optical Parametric Oscillator," in *Conference on Lasers and Electro-Optics,* (Optical Society of America, 2010), pp. TuM6.

12. J. E. Sharping, C. Pailo, C. Gu, L. Kiani, and J. R. Sanborn, "Microstructure fiber optical parametric oscillator with femtosecond output in the 1200 to 1350 nm wavelength range," Opt.Express 18, 3911-3916 (2010).

Students supported during the reporting period:

1. Chenji Gu (planning to defend his PhD dissertation during the fall of 2012).
    a. Centrally involved in the implementation and study of all three light sources and output pulse characterization system. (5 semesters of GSR plus project resources)
2. Christiane Pailo (received her Master's degree during the spring of 2010).
    a. Supported (two semesters of GSR plus project resources) to implement the 1000 nm picosecond system and apply the 1000 nm femtosecond system to nonlinear optical microscopy.
3. Leily Kiani (started in fall 2010 and plans to do her qualifier exam during the spring of 2012).
    a. Partially supported (one half semester of GSR plus project resources) to consider the possibility of using soft-glass optical fibers. Centrally involved in fiber characterization.
4. Thompson Lu (started in fall 2011).
    a. Centrally involved in applying the 1000 nm picoseconds system to nonlinear optical microscopy. (Project resources only).

Other scientists supported by this program:

1. Yan-Hua Zhai (during the spring of 2010)
    a. Supported for 3 months to apply the 1000 nm femtosecond system to nonlinear optical microscopy.

2. Jay Sharping (PI)
    a. Paid 2 summer ninths for efforts spread throughout the 3-year program.

Appendix 1: Matlab simulation code for FOPO systems

Listing of the gnlse.m program

```
function [Z, AT, AW, W] = gnlse(T, A, w0, gamma, betas, loss, fr, RT,
flength, nsaves)

%see comments on page 46 of the supercontinuum book




n = length(T); dT = T(2)-T(1);  % grid parameters
V=2*pi*(-n/2:n/2-1)'/(n*dT);     % frequency grid
alpha = log(10.^(loss/10));     % attenuation coefficient
B = 0;
for i=1:length(betas)           % Taylor expansion of betas
    B = B + betas(i)/factorial(i+1).*V.^(i+1);
end
L = 1i*B - alpha/2;             % linear operator
if abs(w0) > eps                % if w0>0 then include shock
    gamma = gamma/w0;
    W = V + w0;                 % for shock W is true freq
else
    W = 1;                      % set W to 1 when no shock
end
RW = n*ifft(fftshift(RT.'));    % frequency domain raman
L = fftshift(L); W = fftshift(W);   % shift to fft space
% === defin function to return the RHS of eq. 3.13
function R = rhs(z, AW)
    AT = fft(AW.*exp(L*z));
    IT = abs(AT).^2;
    if (length(RT) == 1) || (abs(fr) < eps)  % no raman case
        M = ifft(AT.*IT);       % response function
    else
        RS = dT*fr*fft(ifft(IT).*RW);   % Raman convolution
        M = ifft(AT.*((1-fr).*IT + RS)); % Response function
    end
    R = 1i*gamma*W.*M.*exp(-L*z);       % full RHS of eq. 3.13
end
% === define function to print ODE integrator status
    function status = report(z, y, flag)
        status = 0;
        if isempty(flag)
            fprintf('%05.1f %% complete\n', z/flength*100);
        end
    end
% === setup and run the ODE integrator
Z = linspace(0, flength, nsaves);   % select output z points
% === set error control options
options = odeset('RelTol', 1e-5, 'AbsTol', 1e-12, 'NormControl', 'on',
'OutputFcn', @report);
```

```
[Z, AW] = ode45(@rhs, Z, ifft(A), options); %run integrator
% === process output of the integrator
AT = zeros(size(AW(1,:)));
for i = 1:length(AW(:,1))
    AW(i,:) = AW(i,:).*exp(L.'*Z(i));   % change variables
    AT(i,:) = fft(AW(i,:));             % time domain output
    AW(i,:) = fftshift(AW(i,:))./dT;     % scale
end
W = V + w0;
end
```

Listing of the fopo02.m program

```
% this program simulates a FOPO by executing iterations of GNLS
simulations and spectral filtering
% Written by Jay Sharping with initial commented version on 1/15/2010

% house cleaning
clear variation
%close all
%set(axes,'FontSize',18);
noplot=0;

% pulse properties
tpulse=370e-15;                          % pulse duration in seconds

% cavity assumptions
etaloss=0.01;                            % feedback efficiency of the
cavity
npasses=100;                             % number of passes through the
cavity (actually it goes one more)

% pulse parameters
%n = 2^10;
n = 2^13;
%twidth = 6e-12;
twidth = 12.5e-12;
c = 2.998e8;
lamp = 1032e-9;
vp=c/lamp;
T = linspace(-twidth/2,twidth/2, n);
dt=T(2)-T(1);

% fiber parameters
betas = [b2,b3,b4,b5];               % dispersion polynomial as an
expansion around the pump frequency in MKS dimensions

gamma = 0.011;
loss = 0;
% == Raman response
fr = 0.18;
tau1 = 0.0122e-12; tau2 = 0.032e-12;
RT = (tau1^2+tau2^2)/tau1/tau2^2*exp(-T/tau2).*sin(T/tau1);
RT(T<0) = 0;
RT = RT/trapz(T,RT);
% === simulation
nsaves = 5;

w = wspace(T);                           % vector of w values
vs = fftshift(w/(2*pi));                 % used for plotting
tpoints=abs(int32(floor(tshift/dt)));

% spectral filtering
filt = gaussian(vs,filtpos,wfilt);     % create a gaussian filter
```

```
filt=transpose(filt);
filtout = gaussian(vs,-filtpos/2,wfilt);
[vv pp]=max(filtout);
szfo=size(filtout);
if filtpos>0
    filtout(1:pp)=1;
else
    filtout(pp:szfo)=1;
end
filtout=transpose(filtout);

wls=vs+vp;
wls=c./wls;

%bp;
betas = [b2,b3,b4,b5];               % dispersion polynomial as an
expansion around the pump frequency in MKS dimensions
gamma = 0.01;                            % fiber nonlinearity in MKS
units

% create the pulse in time and frequency
u0 = sqrt(ppower)*gaussian(T,0,tpulse);     % create a gaussian pulse
%u0=sqrt(ppower)*sech(T/tpulse);
U0 = fftshift(abs(dt*fft(u0)/sqrt(2*pi)).^2); % fft and square to get
the spectrum

% do the first pass through the fiber
[Z, A, AW, W] = gnlse(T, u0, wp, gamma, betas, loss, fr, RT, z,
nsaves);

u=A(nsaves,:);
ufirst=A(nsaves,:);
U = AW(nsaves,:);    % calculate the spectrum of the first pulse

% ** removed by Jay in April to try to implement a new type of
filtering
% apply the filter in the first pass so that the field can go back
through
% the fiber. this makes a complete pass throught the cavity
utilde=fftshift(fft(u));                % fft to get the spectrum
utilde=utilde.*filt;
uhalf=ifft(fftshift(utilde));
% **

uhalf=uhalf*sqrt(etaloss*0.8);

[Z, A, AW, W] = gnlse(T, uhalf, wp, gamma, betas, loss, fr, RT, z,
nsaves);
u=A(nsaves,:);
u0tilde=fftshift(fft(u0));              % calculate the input pulse
spectrum so that it can be added to the filtered version

citer=1;
```

```
% do subsequent passes through the cavity
for k=1:npasses

    % add loss and a fresh pump pulse
    if  tshift>=0
        for hh=1:length(u)-(tpoints+1);
        u(hh)=u(hh+tpoints);
        end
    end
    if tshift<0
        for hh=(tpoints+1):length(u)
            u(hh)=u(hh-tpoints);
        end
    end

    if noplot==0
        figure(1);
        subplot(2,2,1);
        plot(T*1e15,abs(u.^2));
        xlim([-500 500])

        subplot(2,2,2);
        plot(T*1e15,abs(u0.^2));
        xlim([-500 500])

    end

    if max(abs(u.^2))<1e-18;
        if k>25
            break
        end
    end
    if max(abs(u.^2))>10;
        citer=citer+1;
        if citer>15
            break
        end
    end
    utilde=fftshift(fft(u));                % fft to get the spectrum
    utilde=utilde*sqrt(etaloss*0.2);                % incorporate the
loss in in out and cavity coupling
    u1tilde=(utilde+u0tilde);               % add the filtered to the
new pump pulse

    % calculate some intermediate values in case you want to plot them
    U1tilde=(abs(dt*u1tilde)/sqrt(2*pi)).^2; % calculate the power
spectrum in case you want to plot it
    u1=ifft(fftshift(u1tilde));             % ifft in order to obtain
the input field for ssprop

    % propagate forward through the fiber
    [Z, A, AW, W] = gnlse(T, u1, wp, gamma, betas, loss, fr, RT, z,
nsaves);
    u2=A(nsaves,:);
```

```
    variation(k)=sum(abs(u)-abs(u2));        % compare subsequent
outputs to see if the system is converging
    if noplot==0
    % calcuate some intermediate values in case you want to plot them
    U2 = fftshift(abs(dt*fft(u2)/sqrt(2*pi)).^2);   % calculate the psd
after going through the fiber
        subplot(2,2,4);
        plot (wls,10*log10(U0),wls,10*log10(U2),wls,10*log10(U1tilde));
        xlim([600e-9,1700e-9]);
        subplot(2,2,3);
        plot(variation)
    end

    %apply the filter to the output after the forward pass
    utilde=fftshift(fft(u2));                % fft to get the spectrum
    utilde=utilde.*filt;

    % propagate back through the fiber
    uhalf=ifft(fftshift(utilde));
    uhalf=uhalf*sqrt(etaloss*0.8);
    [Z, A, AW, W] = gnlse(T, uhalf, wp, gamma, betas, loss, fr, RT, z,
nsaves);
    u=A(nsaves,:);

%k
end

% prepare to analyze the output after lots of oscillations basically
% extracting the idler
utilde=fftshift(fft(u2));                % ft of the output
utilde=utilde.*filtout;
Utilde=abs(utilde.^2);

uu=ifft(fftshift(utilde));              % inverse transform the output
UU=abs(uu.^2);                          % calculate the temporal
amplitude
UU=UU/max(UU);                          % normalize the temporal
amplitude

    if noplot==0
        figure(3)
        plot(T*1e15,UU)
        xlim([-500 500])

    end

    figure(2)                               % prepare to plot the
output from this pass
    set(gca,'FontSize',16);
    plot (wls*1e9,Utilde);
    xlim([700 1000])
    xlabel('lamp (nm)','FontSize',16)
    ylabel('Output power (au)','FontSize',16)
```

```
jj=2;
ll=1;
for ii=jj:length(UU);
if (UU(ii)-0.5)*(UU(ii-1)-0.5)<=0
           tdif(ll)=T(ii);
           ll=ll+1;
end
end
fwhm=tdif(ll-1)-tdif(1);
```

listing of the Sequence06162011v01.m program

```
clear all
close all
%tshift=400e-15;
lamp=1032e-9;                           % set the pump wavelength
wp=2*pi*2.998e8/(lamp);                 % where in frequency units is
the filter center
bp;
zstart=0.04;
for z=zstart:0.01:0.04
    for tshift=300e-15:50e-15:300e-15;
         for ppower=900/z:20/z:1400/z
            for wfilt=9e12:1e12:9e12
                for filtpos=-50e12:5e12:-50e12
                    fopo02

filname=strcat('power',num2str(ppower),'tshift',num2str(tshift*1e15),'f
pos',num2str(filtpos/1e12),'len',num2str(z*100),'fwidth',num2str(wfilt/
1e12),'.mat');
                    save(filname)
                end
            end
        end
    end
end
```

listing of the bp.m program

```
Dfit=[0,0,-652.58,0.96184,-0.00031499,-2.207e-009];
lamvect=[500:1:1500];
Dvect=(Dfit(3)+Dfit(4).*lamvect+Dfit(5).*lamvect.^2+Dfit(6).*lamvect.^3
);
Dvect=Dvect*(1e-6);
lamvect=lamvect*1e-9;
Betavect=-Dvect.*(lamvect.^2)/(2*pi*2.998e8);
Omegavect=2*pi*(2.998e8)./lamvect;

betaparm = polyfit(Omegavect,Betavect,4);

% btest=betaparm(3)+betaparm(2)*Omegavect+betaparm(1)*Omegavect.^2;
%
btest=betaparm(4)+betaparm(3)*Omegavect+betaparm(2)*Omegavect.^2+betapa
rm(1)*Omegavect.^3;
btest=betaparm(5)+betaparm(4)*Omegavect+betaparm(3)*Omegavect.^2+betapa
rm(2)*Omegavect.^3+betaparm(1)*Omegavect.^4;
%
btest=betaparm(6)+betaparm(5)*Omegavect+betaparm(4)*Omegavect.^2+betapa
rm(3)*Omegavect.^3+betaparm(2)*Omegavect.^4+betaparm(1)*Omegavect.^5;

b2=betaparm(5)+betaparm(4)*wp+betaparm(3)*wp^2+betaparm(2)*wp^3+betapar
m(1)*wp^4;
b3=betaparm(4)+2*betaparm(3)*wp+3*betaparm(2)*wp^2+4*betaparm(1)*wp^3;
b4=2*betaparm(3)+6*betaparm(2)*wp+12*betaparm(1)*wp^2;
b5=6*betaparm(2)+24*betaparm(1)*wp;
```

```
%figure(5);
%plot(Omegavect,btest,'o',Omegavect,Betavect,'-');
```

Appendix 2: Master's thesis of Christiane Pailo

UNIVERSITY OF CALIFORNIA
Merced

Description of Fiber Optical Parametric Oscillators as Laser Sources Applied to Cellular Imaging

A Thesis submitted in partial satisfaction of the requirements
for the degree Master of Science

with emphasis

Biological Engineering and Small-Scale Technologies

by

Christiane Goulart-Pailo

Committee in charge:
Professor Ariel Escobar, Chair
Professor Jina Choi
Professor Rudy Ortiz

December 2010

Description of Fiber Optical Parametric Oscillators as Laser Sources Applied to Cellular Imaging

By

Christiane Goulart-Pailo

The thesis of Christiane Goulart-Pailo is approved, and it is acceptable in quality and form for publication on microfilm and electronically:

.

_____

_____ Wei-Chun Chin

_____

_____Rudy Ortiz

_____

_____Ariel Escobar, Committee Chair

December 2010

Acknowledgments

I would like to express my gratitude for the numerous contributions and support that have made my research endeavors possible. I thank my advisor, Dr. Jay Sharping, for his support, and enthusiasm throughout the course of this project. I would also like to thank my thesis committee members, Dr. Rudy Ortiz, Dr. Ariel Escobar, , for their guidance in my research project. My fellow lab members, in particular Jeremy Sanborn, Leily Kiani and all who contributed with their lab skills, emotional support, and humor through it all. Special thanks goes to, Tessa Pinon for her friendship and encouragement on the times of despair. I want to especially thank Dr. Ariel Escobar's lab for using their laboratory space and for the warm welcoming. Special thanks to Dr. Escobar, who not only provided the lab space but also provided long hours of his busy time with patient tutoring and guidance, not only in the project but as a mentor scientist. I thank Marcia Gutierrez that trained on the techniques that will be used on experiments involving biological samples. I also thank the fellow collaborators at Purdue University at Dr. Ji-Xi Chen's lab for providing laboratory space and resources, and for all members of Dr. Cheng's group with their prompt desire to help.

Most importantly, I would like to thank my family, specially my children, Viniccius and Otavio, for the endless hours of patience and sacrifice that made possible for me to be able to complete this project. I thank my close friends, who are my family here in United States for all their continuous love and support throughout the difficult times. Much gratitude goes to my aunt, Jussara Porto, who has encouraged me and always kept the humor going by replacing a mother's role just like she knows how.

Description of Fiber Optical Parametric Oscillator as a Laser Source Applied to Cellular Imaging

by

Christiane Goulart-Pailo

Abstract

The integration of lasers has advanced imaging and quantitative analysis in the study of biological problems. In this document we describe a class of light sources known as fiber optical parametric oscillators (FOPO). The wavelength tunability of the FOPO system is a fundamental feature for the cellular imaging techniques in perspective. The FOPO converts the wave frequency provided by the pump into two other wave frequencies as its output. The difference between two waves frequencies produced by the FOPO, if corresponding to molecular vibrational transitions, is used to excite specific organic bonds. The current system allows one to probe vibrational transitions between 1050 cm^{-1} and 2220 cm^{-1}. This spectral range allows one to excite C-D bonds, carbon-deuterium bond (2100 cm^{-1}), C-H bonds (1445 cm^{-1}), C=O bonds (1742 cm^{-1}) and others bonds occurring in living cells.

As methods we characterize and compare two FOPO systems based on two different photonic crystal fibers (PCF) and two laser pumps in

order to assess their suitability for cellular imaging techniques. We optimize power, stability, and tunability of the output wavelength. Our characterization includes measurements of spectral tunability and pulse quality.

The results expressed upon comparing of the two systems described in this thesis, showed that the picosecond/long fiber system is superior in terms of usability, average power efficiency, and stability but fails to encompass the full range of wavelengths necessary for the variety of intended applications. In comparison, the femtosecond/short fiber system, delivers superior wavelength tunability and pulse quality at the expense of usability and average power.

We conclude that femtosecond/short fiber OPO system is the most suitable system between the two FOPOs systems explored in this study to be applied to nonlinear microscopy techniques. Coherent anti-Stokes Raman spectroscopy (CARS), which is used for imaging of non-stained biological samples, used as an example of nonlinear microscopy applied as a proof-of-concept experiment. The production and characterization of a laser source such as a FOPO that is able to produce desired wavelengths within the scope of cellular imaging, sets the stage for the use of these systems as an unique, efficient, and compact laser source for research of different cellular imaging techniques.

Table of Contents

List of Figures

Chapter I

Introduction

Introduction

Glass fibers were first fabricated in the 1920's, but it was not until the 1950's that fiber optics come to be. At that time optical fibers suffered from tremendous signal losses (loss > 1000 dB/Km). Fibers became more useful in the 1970s when the loss was reduced to 0.2 dB/km. In 1978 fibers such as PCFs, holey fibers, microstructure fibers and tapered fibers were developed and explored. The structural differences in these fibers are directly related to the optical nonlinear effects and dispersive properties that one may observe when they are employed (Sharping, 2008). The relatively small core size of PCFs enhances the nonlinear effects leading to spectral broadening of ultra short pulses and supercontinuum generation (Agrawal, 1989).

The field of nonlinear optics continues to grow. The nonlinear effects in optical fibers have been a vibrant research area for the past 30 years. Applications of nonlinear effects such as four wave mixing (FWM) are actively being pursued. Four wave mixing is viable for fiber amplifiers and is used for ultrafast signal processing and wavelength conversion (Agrawal, 1989; Sharping, 2002).

Optical parametric oscillators (OPOs) are the current-state-of-the-art for the generation of wavelength-agile short pulsed laser radiation in a tunable and stable range of wavelengths. Standard OPOs are based on

$\chi^{(2)}$ crystals and are pumped by lasers such as Ti-sapphire (Sharping, 2002; Spence 1991) . In spite of the fact that such systems are very useful due to the range of wavelengths produced, they are still expensive and too bulky for some biomedical research studies and clinical settings (Keller, 2003).

Fiber OPOs operate through FWM mediated by the $\chi^{(3)}$ nonlinearity of the glass fiber, in this case a PCF (Sharping, 2008). Four wave mixing when phase-matched is efficient over a bandwidth that can be continuous, tunable, and hundreds of nanometers wide. In this manner, FWM underlies the process where signal gain occurs at wavelengths near to and far from the central wavelength produced by the pump (Sharping, 2002). The system is said to oscillate when the pulses coming in the fiber from the pump overlap temporally and spatially with the pulses fed back from a Fabry-Perot cavity (Sharping, 2010).

Fiber optical parametric oscillators provide the ability to tune and amplify the original wave frequency delivered by a laser source (Spence, 1991). The FOPO's ability to tune and amplify the received wave frequency is due to the PCF's nonlinear effects present in these systems. Lasers are some of the most widely used instruments in engineering, physics, life sciences and chemistry (Eriksson, 2008). The aim of our work is to provide a more efficient and portable laser source at perhaps lower cost to fulfill the extreme importance and need for such systems for cellular imaging and other biomedical research applications.

We hypothesize that FOPOs will provide the range of wavelength tunability, power and stability necessary for their use as a light source for cellular imaging applications.

The experimental results presented later in this document involve pulsed lasers and PCFs. In this chapter, I present the key features of the light source which is used to "pump" the FOPO system and the key features of PCFs used in the FOPO system.

The Laser Pump

Lasers are optical-frequency oscillators, which consist of an amplifier and feedback system. The optical amplifier can be composed of different media such as gas, crystalline, glassy solid material, or liquid. Laser amplifiers contain molecules, atoms or ions, within an active gain medium that are excited by an influx of energy from a ground state into a higher energy level. Hence, this gain medium is pumped with an energy source to produce an amplified output signal with increased power. Optical amplifiers are fed by a continuous flux of energy, which can be maintained either with a continuous-wave (cw) or pulsed laser. Sources of this energy can include electrons within a gas medium, a lamp, an electrical current, another laser in a liquid medium or a semiconductor laser consisting of a crystalline or glassy solid. We can consider a quantum mechanical system containing a sequence of

discrete energy levels named E1, E2, E3, with E1 being the lowest energy state and E3 as the highest energy. If a particle is excited to a level E3, such particles then will be transferred to or will excite other particles in a lower level of energy; E2. If the number of particles, molecules or ions in an E2 energy level is larger than the population in the E1 energy level, thus a population inversion occurs. If the system is capable of amplifying radiation of frequency $\hbar\nu = E2 - E1$, where $\hbar$ is the Planck's constant, the system is considered ideal (Verdeyen, 1994).

Resonator

The optical resonator within a laser system provides feedback of light and stimulates oscillation. Some laser systems such as the Nd:YAG system used in this study, uses a Fabry-Perot cavity in which two mirrors are arranged parallel to one another. The light reflects back and forth between the two mirrors and passes multiple times through the optical amplifier. This process reinforces the oscillation and transforms the amplifier into an oscillator. One of the mirrors must be partially transmitting to permit the output beam to leave the cavity. The choice of mirrors utilized in this process depends on the laser type and its gain (Moore, 2003).

The femtosecond fiber laser that we use in this study employs a ring cavity. The ring is composed of a fluorozirconate fiber (Silica/Fluoride)

doped with Yb^{+3} (Yetterbium). The fibers are connected together in a ring. The laser system also includes a polarization control. A ring cavity is advantageous to use as a pulse laser source because only the threshold peak power undergoes complete transmission by one of the rings that serves as coupler. Therefore, the laser is referred to be functioning at mode locked operation. (Verdeyen, 1994).

Moreover, lasers will oscillate only if the gain is larger than all the losses in the system such as transmission losses, absorption, scattering at the mirrors, and any loss of the amplifier medium itself (Verdeyen, 1994).

In the order to calculate the expected parameter values for the hardware to achieve optimum modes of operation, we considered an ideal laser system which allows larger gain than the loss in the system. Example of modes include; the spatial mode (spatial shape of the pulse), temporal mode (temporal width of the pulse), and center wavelength. The laser will work best in certain modes of operation because these modes are solutions for Maxwell's equations (expanded in chapter two), which is dependent on the hardware employed for the specific system. However, power saturation of the output might occur. (Sharping, 2009).

Photonic Crystal Fibers, PCF

The PCF is a fundamental component of the FOPO system and affords the unique ability to change the dispersion, thereby generating a range of tunable wavelengths. The silica material in a PCF is distributed in a matrix manner where the air holes size and the hole-pitch size affect both the linear and nonlinear optical properties of the fiber (NKT Photonics, 2009).

The core of an optical fiber has an effective refractive index (n_{eff}) larger than the refractive index of the cladding of the fiber. The structure is shown in Figure 1.1. The effective refractive index of the PCF is related to the propagation constant k_0 defined for the propagation of light in free space (Agrawal, 2007):

$$k_o = \frac{2\pi}{\lambda} \tag{1.1}$$

where λ is the wavelength. For light propagating in a material such as glass, the propagation constant will be given by:

$$k = \frac{2\pi n}{\lambda} \tag{1.2}$$

where n is the refractive index, and since as mentioned above the refractive index will vary from the core of the fiber to the cladding of the fiber, the propagation constant will then also vary. Therefore we will have:

$$\frac{2\pi n_{cl}}{\lambda} < \frac{2\pi n_{eff}}{\lambda} < \frac{2\pi n_{cr}}{\lambda} \tag{1.3}$$

$$k_{cl} < k_{eff} < k_{cr} \tag{1.4}$$

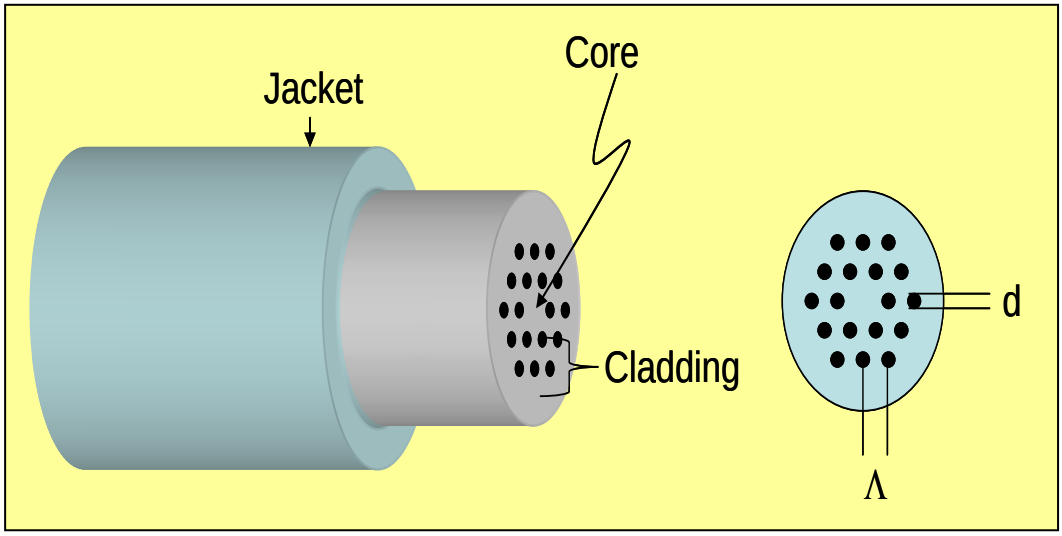

Figure 1.1 Schematic of the classical triangular cladding single-core photonic crystal fiber in which light is guided in a solid core embedded in a triangular lattice of air holes. The fiber structure is determined by the hole-size, d, and the hole-pitch, Λ. The PCF is coated with a high index polymer for protection.

Here n_{cr} is the refractive index of the PCF's core, n_{cl} is the refractive index of the PCF's cladding, and n_{eff} is the effective refractive index of the fiber. Therefore, the nomenclature for the propagation constant also follows in the same manner. The electric field distribution as it propagates through the PCF's core and cladding will define the effective propagation constant, k, of the transverse electric field going through the fiber as (Hecht, 2002):

$$E(\omega, t) = A(\omega, t)\sin(\omega_0 t - \phi(\omega, t)) \qquad (1.5)$$

Equation 1.5 can be manipulated to be written as:

$$E(z, t) = A\exp(kz - \omega t) \qquad (1.5)$$

where A is the amplitude of the electric field, ω is the angular frequency, ϕ is the phase angle, t is the total time, and z is the axis of propagation. The propagation of the transverse electric field in a guided medium such as a PCF will have a propagation vector defined as (Hecht, 2002):

$$\beta = n_{eff}\, k = \frac{n_{eff}\, 2\pi}{\lambda_o} \qquad (1.6)$$

The propagation of the light beam within the fiber and its interaction with the structure of the PCF brings the center wavelength to temporally and spatially disperse itself. The velocity by which the pulse envelope the overall shape of the wave's amplitude travel through the fiber, is referred to as group velocity GV. The GV of light in a PCF can be calculated by taking the first derivative of the

phase mismatching of these wave frequencies $\Delta\beta$. The second derivative of the phase mismatch curve describes the zero wavelength dispersion in the PCF. If the laser center wavelength is near to the zero dispersion wavelength of the PCF, the phase matching condition is more likely to be met. Thus, the FWM process that underlies the FOPO systems described here will be promoted (Marhic, 2008).

In conclusion, we chose 1 μm wavelength for this investigation because this wavelength transmits reasonably well through living tissues. The PCFs used in the FOPO systems described in this thesis possess suitable mode propagation vector ($\Delta\beta$) that facilitate the phase matching condition necessary for efficient FWM process to take place.

Chapter II

Electro Magnetic Description of Pulse Propagation, Four Wave Mixing in Fiber OPO

In this chapter we explore the theoretical aspects of the gain profile and what influences efficient wavelength conversion produced by FOPO systems, with FWM as the underlying process. The FWM process will take place within a PCF. In order for the FWM process to take place efficiently, two conditions must be met; momentum and energy conservation described in the mathematical expressions below:

$$\Delta\beta = \beta(\omega_s) + \beta(\omega_p) - 2\beta(\omega_p) = 0 \tag{2.1}$$

$$2\omega_p = \omega_s + \omega_i \tag{2.2}$$

where β is the propagation vector, and ω_p, ω_s and ω_i are the pump, signal and idler's angular frequencies respectively.

In order to oscillate the gain of the system given by the equation below, gain must be larger than the loss of the system:

$$G = 1 + \left[\gamma \frac{P_p}{g} \sinh(gL) \right]^2 \tag{2.3}$$

where G is the total gain of the system, P_p is the pump power, g and γ is defined later in this chapter, and L is the fiber interaction length.

In order to further clarify the terms and their importance on the equations above to describe the gain profile, a more detailed explanation is given in the rest of this chapter (Hansryd, 2002).

Pulse Propagation

Maxwell's equations regulate the propagation of optical field in free space as well as in a guided medium. Therefore, for free space we have (Agrawal 2000):

$$\nabla \times E = \frac{\partial B}{\partial t} \quad (2.4)$$

$$\nabla \times H = J + \frac{\partial D}{\partial t} \quad (2.5)$$

Electric (E) and magnetic (H) field vectors, where J, current density is 0 when the optical field is propagating in free space

$$\nabla \bullet D = \rho_f \quad (2.6)$$

$$\nabla \bullet B = 0 \quad (2.7)$$

The electric (D) and magnetic (B) flux densities, where ρ_f is 0 for free space propagation

The Fiber

The mathematical description of the propagation of light through free space of the pulses originated at the pump brings us to the mathematical description of light pulses in a medium such as an optical fiber. However, such a mathematical description needs to take into account the physical effects, nonlinear response, of the medium in this case the PCF. The medium's nonlinear response is due to the non harmonic motion of bound electrons under the influence of intense electric field. These bound electrons then produce electric dipoles, which will in turn affect the electric field polarization, P:

$$P = \varepsilon_o\left(\chi^{(1)} \cdot E + \chi^{(2)} : EE + \chi^{(3)} \vdots EEE + ...\right), \quad (2.8)$$

where ε_0 is the permittivity constant, and $\chi^{(j)}$ is the susceptibility tensor of rank (j+1). The second order susceptibility tensor $\chi^{(2)}$ is responsible for the second harmonic generation. However, in the case of silica glasses (SiO_2) this second order susceptibility tensor effect disappears due to the symmetry of such a material. The most important nonlinear contribution is due to the third-order tensor $\chi^{(3)}$, which is responsible for third-harmonic generation, FWM, and nonlinear refraction (Agrawal, 2007).

These nonlinear processes, generate new frequencies that, when phased matched, are efficient produced and result in new wavelengths generated within the optical fibers.

Brief description of Nonlinear Pulse Propagation in Silica Fiber

Consequently, taking into account the nonlinear effects resulting from the fiber composition we can manipulate Maxwell's equations in order to describe the propagation of light in a medium such as an optical fiber. We observe that the flux densities arising from the propagation of E, the electric field, and H, the magnetic field, in a medium are connected using the following constitutive relations:

$$\begin{cases} D = \varepsilon_{\circ} E + P \\ B = \mu_{\circ} H + M \end{cases}$$

, where $\varepsilon_{\circ}$ is the permitivity constant in vacuum and μ_0 is vacuum permeability constant in vacuum. P and M are the polarization of light due to the electric field and to the magnetic field respectively. M is zero for mediums such as fibers

(2.9)

(2.10)

Therefore, substituting D into equation 2.5

And knowing that J=0 $\quad \therefore \nabla \times H = \frac{\partial \varepsilon_{\circ} E + P}{\partial t}$ (2.11)

$$\nabla \times H = \frac{\partial \varepsilon_{\circ} E}{\partial t} + \frac{\partial P}{\partial t}$$

Now, using equation 2.4 and substituting the magnetic field (B) by equation 2.10

$$\nabla x E = \frac{\partial B}{\partial t}$$

$\therefore \nabla x E = \frac{\partial \mu H}{\partial t}$, substituting δH by equation 2.11

and using $\varepsilon_0 \mu_0 = 1/c^2$ we arrive to:

$$\nabla x \nabla x E = \frac{1}{c^2} \frac{\partial^2 E}{\partial t^2} + \frac{\mu_0 \partial^2 P}{\partial t^2} \quad (2.12)$$

Thus, the nonlinear response effect in pulse propagation in a fiber can be described basically by the derivation of the equation below; it will influence the shape as well as the spectra of these short pulses (Agrawal, 2007, 27):

$$\nabla x \nabla x E = -\nabla^2 E \quad (2.13)$$

$$\frac{1}{c^2}\frac{\partial^2 E}{\partial t^2}+\frac{\mu_0\partial^2 P}{\partial t^2}=-\nabla^2 E \qquad (2.14)$$

We can use the mathematical description of the polarization in equation 2.8. Assuming that the nonlinear portion of the polarization is small, one can also write this equation as (Agrawal, 2007, 26):

$$P(r,t)=P_L(r,t)+P_{NL}(r,t), \qquad (2.15)$$

P_L is the linear portion of the polarization and P_{NL} is the nonlinear portion of the polarization.

Substituting the polarization portion by equation 2.14 and through algebraic steps we have:

$$\frac{\mu_0\partial^2 P_L}{\partial t^2}+\frac{\mu_0\partial^2 P_{NL}}{\partial t^2}=\nabla^2 E-\frac{1}{c^2}\frac{\partial^2 E}{\partial t^2}, \qquad (2.16)$$

assuming that the nonlinear portion is just a small perturbation and that the overall polarization will not change a scalar multiplication of the original polarization is a valid description. When the range of frequencies in a pulse envelope varies by a very small amount, the optic field is said to be quasi-monochromatic (Agrawal, 2007, 32).

The Parametric Process: Four Wave Mixing

The nonlinear aspect of the polarization can be considered by understanding the basic principles of FWM effects as a response of

the bound electrons of a material such as an optical fiber, to an intense electric field. This process is referred as a parametric process because it is produced from the modulations of light in a fiber as a consequence of fiber parameters, such as the refractive index. The FWM process can be explained as the interaction of four stationary copolarized waves going through a fiber and the nonlinear process originated due to the interaction of these wave frequencies. Everything starts with two wave frequencies (ω_1, ω_2), beating with each other continuously through a PCF, which will in turn modulate a resultant frequency for example $(\omega_3 \pm (\omega_2 - \omega_1))$. The nomenclature used for these frequencies is presented in the literature as (ω_1, ω_2) for the starting waves, being (ω_3) assign to the frequency of the laser pump. The interaction of (ω_3) with (ω_1, ω_2) can result in wave frequencies such as $(\omega_4 = \omega_2 \pm (\omega_3 - \omega_1))$ called the idler, a wave that is shorter then laser pump center wavelength, but carries a larger amount of energy. The combination of the two wave frequencies (ω_1, ω_2), beating with each other, with the laser pump frequency (ω_3) can also result in a wavelength band that is longer in terms of wavelength carrying a smaller amount of energy than the pump center wavelength band (Hansryd, 2002).

Therefore, if FWM is polarization dependent and if one generally assumes that the four waves are linearly polarized and

travelling through the fiber the total transverse field E(x,y,z) can be described as (Marhic, 2008):

$$E(r,t) = \frac{1}{2}\hat{x}\sum_{j=1}^{4}[Ej[i\exp(\beta_j z - \omega t)] + c.c.] \quad (2.17)$$

$\hat{x}$ is the unit vector and $E(r,t)$ is slowly varying portion of the electric field and c.c. is the complex conjugate. Therefore, we can achieve the gain derivation of the FOPO system by expressing the nonlinear portion of the polarization in the same form as equation 2.3 by taking the second derivative in respect to time and space of the resultant equation 2.17 above (substituted into equation 2.15), and after simplifications that are beyond the scope of this thesis:

$$\mathrm{P_s(L) = P_s(0)}\left(1 + \left[\frac{\gamma \mathrm{P_p}}{\mathrm{g}}\sinh(\mathrm{gL})\right]^2\right) \quad (2.18)$$

$$P_i(L) = P_i(0)\left(\left[\frac{\gamma P_p}{g}\sinh(gL)\right]^2\right) \quad (2.19)$$

This equations are analytical solution derived in the process of the gain equation, where $\mathrm{dA_0/dz = 0}$, A is the amplitude of the electrical field going through the PCF in the z direction, L is the fiber interaction length, $\mathrm{P_i}$ and $\mathrm{P_s}$ are the power of the electric field carried by the idler and the signal respectively, γ is the fiber nonlinear coefficient, and g is the parametric gain coefficient given by (Hansryd, 2002):

$$g^2 = [(\gamma P_p)^2 - (\kappa/2)^2] = \Delta\beta[\frac{\Delta\beta}{4} + \gamma P_p] \quad (2.20)$$

In this equation, κ is defined as $\kappa = \Delta\beta + 2\gamma P_p$, where $\Delta\beta$ is the linear phase mismatch.

Thus, using the previous equations we can achieve the gain equation: (Hansryd, 2002):

$$G = \frac{P_s(L)}{P_s(0)} = 1 + \left[\frac{\gamma P_p}{g}\sinh(gL)\right]^2 \quad (2.21)$$

Fiber properties such as the nonlinear coefficient γ will influence the light output due to the response of the silica atoms to the light beam within the fiber. The phase mismatch between the four waves going through the PCF can only disappear if all four wave frequencies and wave vectors are matched as mentioned in chapter one.

One can also explain FWM process in quantum-mechanics terms as when the two photons from the pump laser are annihilated and two new photons are created in a pattern that allow energy and momentum conservation, as the equation describes, through the interaction with parameters such as the refractive index of the fiber as illustrated in Figure 2.1 (Marhic, 2008).

$$\omega_3 + \omega_4 = \omega_1 + \omega_2 \quad (2.22)$$

Moreover, the difference between wave propagation vectors must be equal to zero in order to fulfill the energy and momentum conservation of the above as (Marhic, 2008):

$$\Delta\beta = \beta_3 + \beta_4 - \beta_1 - \beta_2 = 0 \tag{2.23}$$

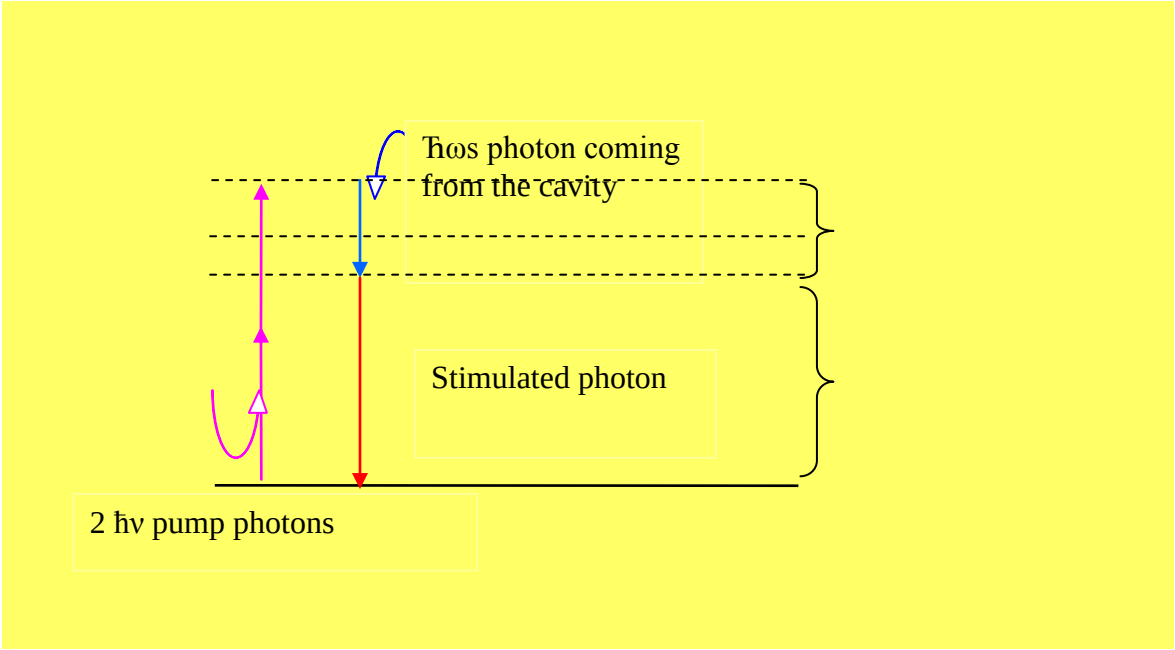

Figure 2.1. An illustration of the four wave mixing (FWM) process. The FWM process can be explained, as seen in this figure, as the interaction of two photons carrying the same amount of energy, coming from the pump and going through a PCF. Due to the nonlinearity of the PCF, these photons interact in such way that an idler in orange and the signal photons in blue are produced. The idler at smaller wavelength carries more energy, than the signal at longer wavelength. Moreover, as conservation of energy and momentum dictates the pump photons' energy and momentum equals the summation of energy and momentum carried by the idler and signal photons produced.

Conclusions

The integrated PCF and FOPO systems in this investigation were chosen for the tunable wavelengths they can generate. In particular, the PCF utilized in the FOPO system provides novel dispersion properties compared with conventional fibers and offers enhanced nonlinear optical effects. In this chapter, we explored the linear and nonlinear polarization effects present in FOPO systems. The effect of the PCF parameters such as nonlinear coefficient γ, and the fiber zero dispersion wavelength influences the electric field propagating through this fiber. The phase mismatch $\Delta\beta$ is a result of this interaction. Thus when phase matching of the waves going through the fiber is achieved, $\Delta\beta=0$, the mathematical expression in equation 2.1 verifies that momentum and energy conservation conditions have been met to achieve efficient amplification of the wave frequencies formed in the FWM process.

In general, if the gain increases, the tunable range of wavelengths will decrease. If phase matching is fulfilled, with the system achieving a larger wavelength tunability range, the gain will decrease. Therefore, the FOPO output of interest will restrict the choice of fiber parameters (fiber length, nonlinear coefficient, core diameter and zero wavelength dispersion) and laser pump parameters

(power, pulse duration, and central wavelength), as seen in equation 2.3, because the gain of the system needs to be larger than its loss in order to efficient amplification of the FOPO output to take place and in order to minimize the loss of wavelength tunability.

Chapter III

Picosecond-Long Fiber OPO's Stability and Tunability for Cellular Imaging Application

Introduction

Since the 1990's, a whole new series of microscopy techniques has flourished. Biomedical applications involving the excitation of organic and inorganic samples were performed for kinetic and imaging studies (Cheung, 1990). Widespread success of a diverse array of microscopy techniques such as two photon fluorescence (TPF), coherent anti-Stokes Raman scattering (CARS), or stimulated Raman scattering, (SRS) are not just limited by the development of equipment such as confocal microscopes, but by the light sources which the technique depend upon (Evans, 2005). The laser sources available are relatively expensive, bulky and it is likely that more than one laser source is required to satisfy the imaging requirement (Eriksson, 2008; Evans, 2005). In this chapter we describe an alternative laser source; a fiber optical parametric oscillator (FOPO) implemented using a mode-locked 1064 Nd:YAG and 1.4 m long photonic crystal fiber. Images of cells, tissues, and drug delivery systems using high-speed vibrational modes of bonds require that the energy of the bond needs to be matched with the laser outputs' frequency separation in order for the imaging acquisition, such as CARS, to take place (Chen, 2010; Cheng, 2008). In the case of FOPO the energy necessary to excite a bond is obtained by the energy difference of two of the energy bands of the FOPO output.

For example, table 3.1 illustrates typical stretching bonds' modes used to produce images using techniques such as CARS. Table 3.1 also illustrates the required FOPO output using the system described in this chapter.

Our hypothesis is that the FOPO pumped by picosecond pulses and implemented with long PCF will generate tunable radiation and power at the wavelength of interest.

Table 3.1

Typical Bond's Stretching Modes for CARS and Corresponding FOPO's Output				
Bonds	**Energy Necessary for bond Streching in Wavenumber (cm^{-1})**	**FOPO's laser Pump wavelength (nm)**	**FOPO's Output Signal (nm)**	**FOPO's Output Idler (nm)**
C-D	**2100**	**1064**	**1370**	**870**
C=C	**1654**	**1064**	**1291**	**905**
CH_3	**2935**	**1064**	**1545**	**811**
CH_2	**2850**	**1064**	**1527**	**816**
=CH	**1265**	**1064**	**1230**	**933**
C=O	**1742**	**1064**	**1307**	**897**

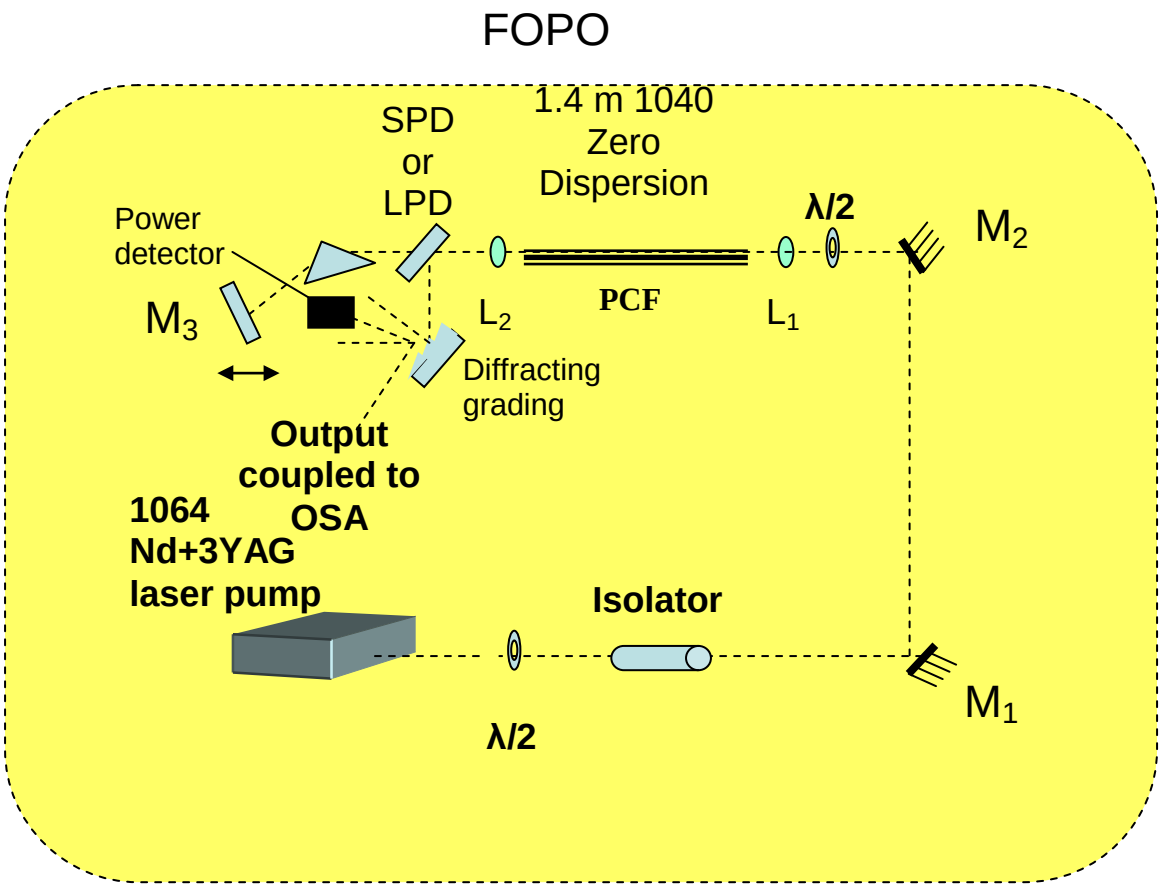

Fig 3.1 Schematic of the FOPO employing a ps Nd:YAG laser that emits an 80 MHz train of pulses at a center wavelength at 1064 nm. The FOPO is a Fabry-Perot cavity formed between one end of the PCF and a metallic mirror (M3). The output coupler is a short-pass dielectric (SPD) or a long-pass dielectric (LPD) that reflects wavelengths longer or shorter than the pump and transmits shorter or longer wavelengths to the cavity.

Methods:

The proposed FOPO setup is shown schematically in Figure 3.1. Light from a Nd:YAG laser is coupled into the 1.4-m-long PCF. Half wave plates (λ/2) are included for polarization control and control of the power launched into the system. A Fabry-Perot cavity is formed between the end surface of the PCF and a gold mirror mounted on a translation stage required for the adjustment of the cavity length. The PCF is 1.4 m long with zero dispersion wavelength at 1060 nm. Aspheric lenses (C110TME-C, .40NA Thorlabs, Inc.) with a working distance of 3.39 mm are used to focus the beam into the PCF and to couple the beam into the cavity. A maximum of about 600 mW of average power can be delivered through the fiber. We typically obtain a maximum total coupling efficiency of ~60%. In order to align the system, we reduce the power and deliver the beam into the PCF using mirrors M_1 and M_2. The beam must hit the middle of each mirror and the alignment should be checked with the help of an IR viewer or IR card. In order to achieve efficient coupling, it is critical to make the necessary adjustments to the mirror (horizontally and vertically) so that the beam is leveled at the same height across the cavity. After coarse adjustments, the light beam can usually be detected on the IR card at the output of the fiber as a homogeneous focused circle and fine

adjustments can be made in order to maximize power. The alignment of the Fabry-Perot cavity is performed by adjusting the position and orientation of the cavity end mirror, M_3. If the cavity is aligned spatially, a back reflection filtered by the isolator is observed on an IR card. A prism is placed between the second lens L_2 and the end mirror M_3 in order to introduce dispersion and therefore improve tunability over the wavelength range of interest. In this case, the output coupler is a short-pass dicroic mirror which was placed between the second lens and prism so that wavelengths longer than that of the pump are reflected out the cavity. The short wavelengths oscillate in the cavity.

Fiber Properties

To obtain the optimum results, a 1.4 m of commercially available SC5.0 1040 zero dispersion fiber was used to construct the FOPO. This fiber is described by the manufacturer, NKT Photonics, as a pure silica photonic crystal fiber with a cladding diameter of 125 $\pm 3\mu m$ coated with acrylate with a diameter of $244 \pm 10 \mu m$ and core diameter $4.8 \pm 0.2\mu m$ (NKT Photonics, 2009). The nonlinear coefficient of this fiber is γ=11 $(W.km)^{-1}$ at 1040 nm zero wavelength dispersion and the fiber experiences a single fundamental mode

through the wavelength range from 400 nm to 1500 nm approximately.

The Laser Pump

As mentioned above, the pump laser is an Nd:YAG laser. It was chosen for the experiment due to its relative long pulse duration (7.9 ps) resulting in a peak power of approximately 1 kW. This power and repetition rate means that one can implement the FOPO system using a PCF with a length approximately corresponding to the repetition rate of the pump laser. The output wavelength of 1064 nm is appropriate to obtain tunable oscillation over a reasonable large range of wavelengths useful for cellular imaging.

Analysis Methods

We use an optical spectral analyzer (OSA) to characterize the output from the FOPO. The OSA allows us to plot the output spectrum for different central wavelengths and pump powers. In the measurements of the Stokes peak, the FOPO's long wavelength output versus the power (W) of the laser pump beam we used a power meter placed before the SPF and after the PCF respectively, as seen in figure 3.2. The wavelength is tuned by shifting the position

and orientation of M_3. As a result, the Stokes band moves away or towards the pump center wavelength depending on the alignment. Our procedure consists of measuring the output spectrum and average power for different pump peak powers and output wavelengths.

Results

Figure 3.2 shows optical spectra recorded at the output of the FOPO. From this plot one observes that the system operates over a wavelength range of about 1090 nm up to 1120 nm. The output power varies over this range by at least a factor of five. The spectral width of the output is 2 ± 1 nm. The noise below -64 dBm is the noise level of the OSA, and not the noise due to the FOPO. The system delivers considerably lower power near 1120 nm; reaching its limit of wavelength tunability.

As shown in figure 3.3, plots of power as a function of wavelength reveal that the FOPO output behaves in such way that as the wavelengths increases, the power increases to reach a maximum, and then decreases rapidly on the long wavelength side of the curve. These behaviors can be noticed through the slopes of the power curves, especially on the curve plotted using experimental values. In addition, the maximum output power increases as pump power increases, as does

the wavelength corresponding to the peak power. In this experiment we were able to obtain a record power for a FOPO long wavelength output of 100 mW.

In addition, we experimentally observe that the system is easy to align and remained stable. The output power fluctuates by only 2% over several minutes. Moreover, the system supports configuration modification with minimal necessary alignment procedures to restore oscillation.

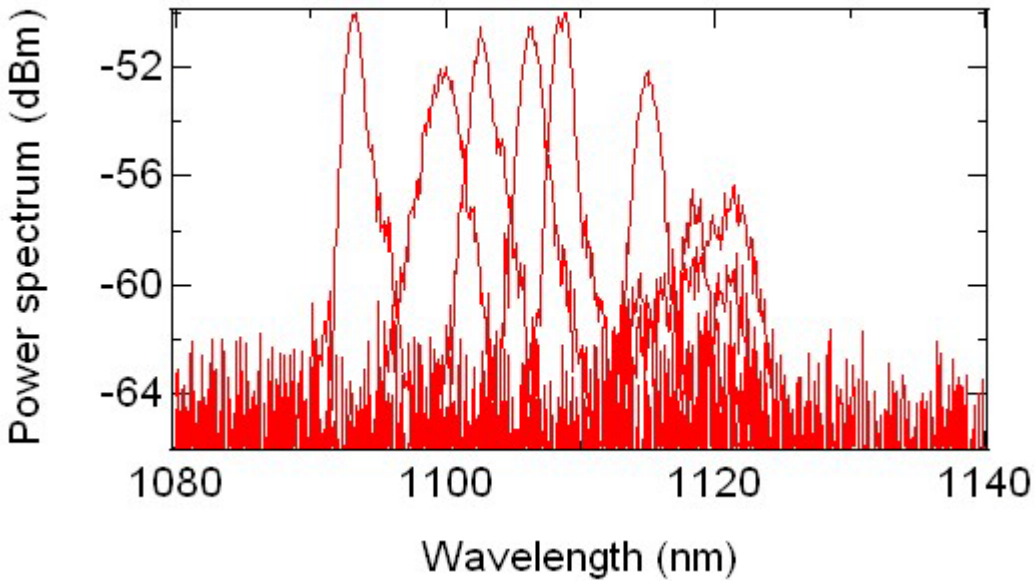

Fig 3.2 A composite of output spectra obtained for a FOPO pumped by a mode-locked Nd:YAG with a repetition rate of 80-MHz, and 1064 nm center wavelength. In this spectrum the power varies across the range of wavelength tunability, where the maximum power is a wavelength of ~1095 nm.

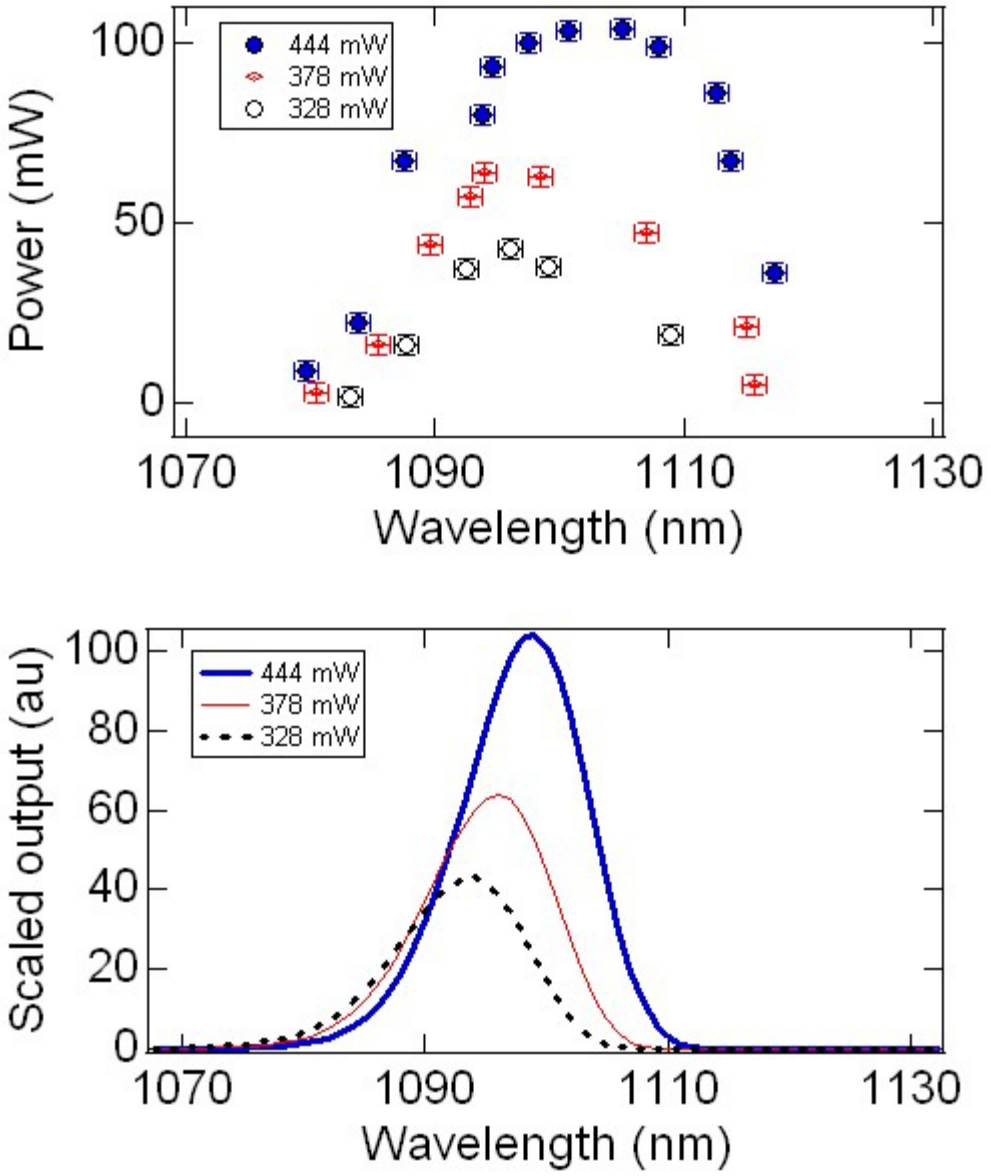

Fig 3.3 A) Plots of measured output power as function of wavelength for different pump powers
B) Calculations of the expected output as a function of wavelengths for different pump powers

Discussion

In chapter two, the results of our calculations presented the tunability of the FOPO output peaks produced by FWM is achieved by the laser pump and PCF characteristics. The PCF length is determined by the laser pump center wavelength of operation (1064 nm) and the laser pump repetition rate (80 MHz). The fiber constitution such as the effective refractive index and the PCF core size influences the phase matching, critical for oscillation of the system. The zero dispersion wavelength of the fiber also determines effects such as phase matching. The available fiber used in this experiment has a zero dispersion wavelength of 1040 nm, which is not the ideal value for this system given that the laser pump center wavelength is 1064 nm. The problem arises because phase matching becomes difficult to obtain if the center wavelength of the laser pump greatly differs from the zero dispersion wavelength of the PCF.

The system used in this experiment is capable of producing FWM output tunable at the long wavelength band but not tunable at the short wavelength band. In addition to FWM there is a Raman effect that must be considered in order to explain the behaviour of the system. As shown in Figure 3.4, FWM and Raman do not behave the same on both sides of the pump peak. When the system is configured to obtain long wavelengths at the output, the gain due to

FWM is accompanied by the gain due to Raman scattering. The energy shifted to short wavelengths due to FWM gets recycled into the pump due to Raman loss. On the other hand, when the system is configured to obtain short wavelength at the output, the energy shifted to short wavelengths by FWM is shifted back to the pump via Raman scattering. Thus, the output is suppressed. In summary, for long wavelengths Raman and FWM cooperate and for short wavelengths, Raman and FWM compete.

The enhanced stability of this system is due to several factors that are related to its configuration and the laser pump. For example, the stability is increased by maintaining the beam at low position, and using as few mirrors as possible in order to direct the light throughout the system. We also infer that the laser pump greatly contributes to the stability of this system compared to the other system presented in this study. First, the Nd:YAG laser is a mature technology long available in the market. Second because Nd:YAG lasers offer a longer pulse duration, ps, compared to the other system which has a shorter pulse duration, 300 fs. The longer pulse duration gives a larger temporal tolerance in terms of alignment of pulses, and the system is more likely to oscillate.

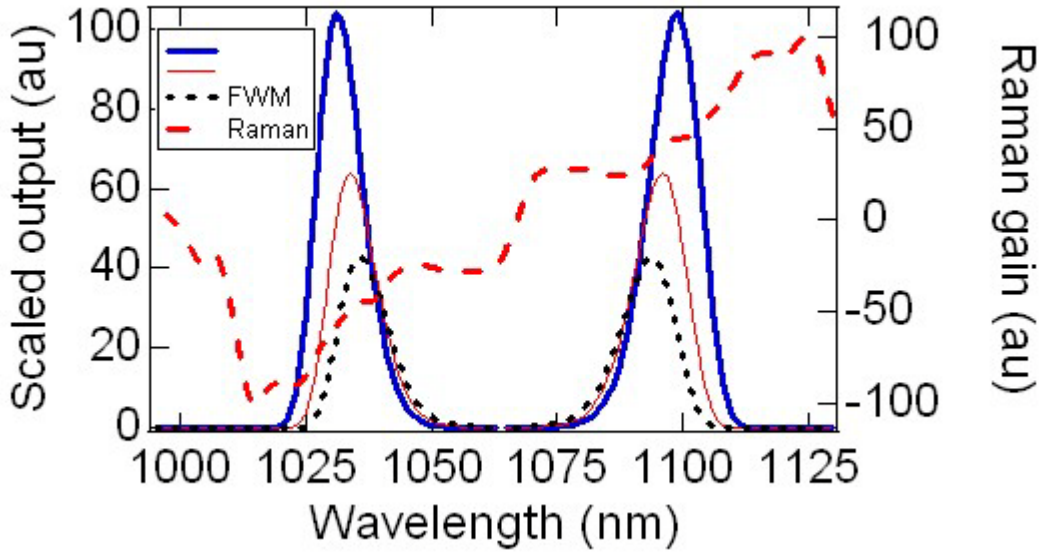

Fig 3.4 This figure shows a comparison between FWM gain and Raman gain. The main feature is the FWM gain being positive on both sides of the pump wavelength of 1064 nm. The Raman gain, on the other hand, is positive for the long wavelength side and negative for the short wavelength side. On the long wavelength side FWM and Raman cooperate. On the short wavelength side FWM and Raman compete.

Conclusions

We conclude that the system presented in this chapter offers stable and reliable output with a record power for FOPO of 100 mW suitable for applications that do not require a large tunable wavelength range. However, the tunable range presented here, 1090 nm to 1120 nm (wavenumber 200 cm^{-1} to 450 cm^{-1}) does not correspond to the typical bond stretching modes for the applications for which this system is envisioned to be applied. In spite of this fact, the stability and high power makes it suitable for biomedical settings.

Chapter IV

Femtosecond-Short Fiber OPO's Stability and Tunability for Cellular Imaging Applications

Introduction

Wide wavelength tunability is fundamental for applications in cellular imaging studies. The system described in the previous chapter used a long fiber and long pump pulses. In this chapter we hypothesize that a short modified PCF and shorter pump pulse duration result in a more widely tunable system compared with the ps system described in the previous chapter (Goulart-Pailo, 2009).

Methods

The proposed FOPO setup is shown schematically in Figure 4.1. The light is coupled into the 3-m-long Fabry-Perot cavity. Half wave plates ($\lambda/2$) are included for polarization control and for control of the power launched into the system. The PCF is ~ 3 cm long with a zero dispersion wavelength at 1030 nm. Aspheric lenses (C230TMeB Thorlabs, Inc.) with a working distance of 2.00 mm are used to focus the beam in to the PCF.

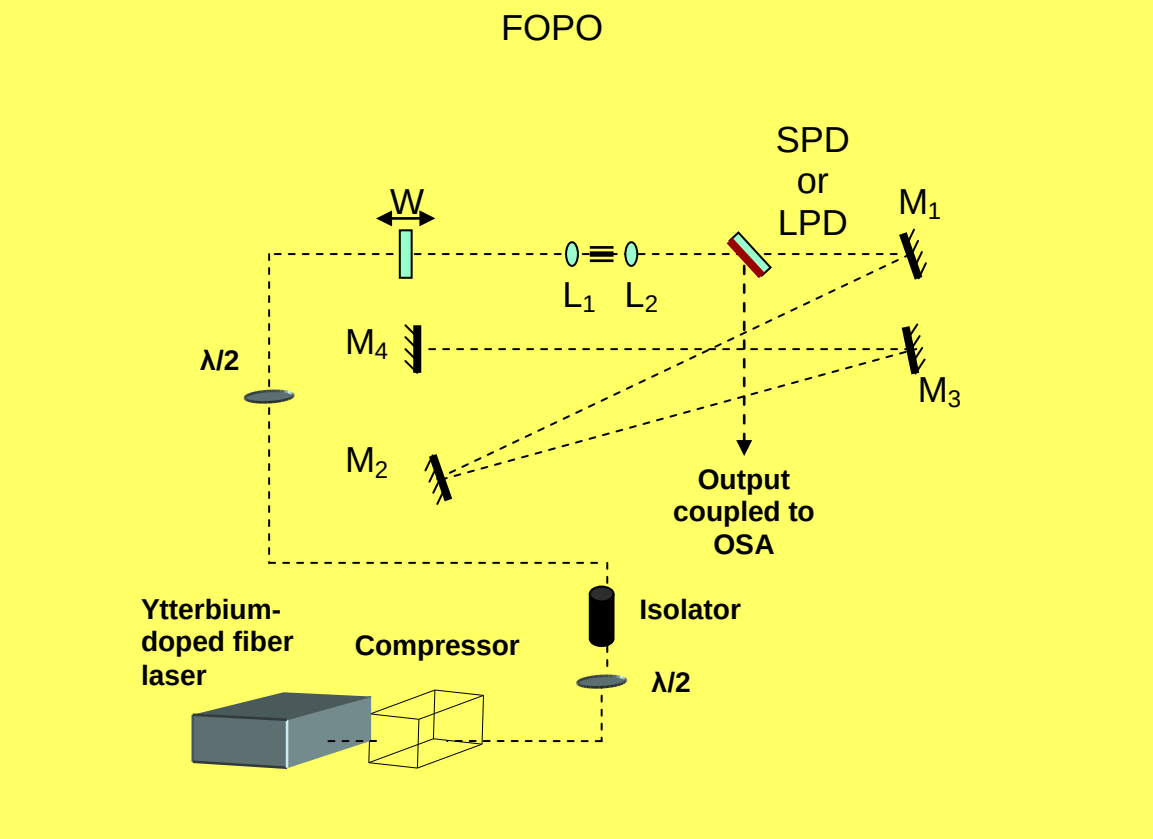

Fig 4.1 Schematic of the FOPO employing a fs Ytterbium doped fiber laser (Polaronix-Uranius), that emits a 50 MHz train of pulses and 1032 nm center wavelength. The FOPO is a Fabry-Perot cavity formed between a glass slide (W) and a metallic mirror (M_4). An output coupler is a short-pass dielectric (SPD) that reflects wavelengths longer than 1100 nm and transmits shorter wavelengths, or a long-pass dielectric that reflects wavelengths shorter than 950 nm.

A maximum average power of about 1.2 W can be delivered through the fiber. We typically obtain a maximum total coupling efficiency of ~60%. In order to align the system, we reduce the power and deliver the beam into the PCF using mirrors M_1, M_2 and M_3. The beam should hit the middle of each mirror and one should check the alignment with the help of an IR viewer or IR card. In order to achieve efficient coupling, it is critical to make necessary adjustments, to the mirror (horizontally and vertically) so the beam is leveled at the same height across the cavity. After coarse adjustments the light beam can usually be detected on the IR card at the output of the fiber as a homogeneous focused circle, and fine adjustments can be made in order to maximize power. The alignment of the Fabry-Perot cavity is performed by adjusting the position and orientation of the cavity end mirror, M_4. If the cavity is aligned spatially, one observes a back reflection filtered by the isolator, which can be observed on an IR card. The output coupler is a short-pass (SPD) or long pass (LPD) dichroic mirror which is placed after the second lens so that wavelengths longer or shorter than the pump are reflected out the cavity, respectively. For example, if the SPD mirror is used the short wavelength bands will oscillate in the cavity and the long wavelength bands will be filtered

out of the Fabry-Perot cavity. Comparably, the opposite will occur if LPD mirror is used.

Fiber Properties

The length of PCF used was 3 cm (Crystal Fiber - SC 5.0) with the zero wavelength dispersion originally at 1040 nm. The PCF had its core reduced in diameter using a flame-brush tapering from a 6 μm to a 4μm apparatus, which resulted on the reduction of the zero wavelength dispersion to 1030 nm. Therefore, the wavelength tunability is expected to increase due to the laser pump's center wavelength proximity to the zero wavelength dispersion of the PCF.

Laser Pump Properties

As mentioned above, the pump laser is an 370-fs, 50-MHz mode-locked Ytterbium-doped fiber laser (PolarOnyx - Uranus) laser. It was chosen for this experiment due to the relatively short pulses (300 fs) with desired center wavelength. The average laser power, pulse temporal duration and laser center wavelength, means that one can implement the FOPO using a short PCF. The center wavelength produced by this laser is 1032 nm

Analysis Methods

We use a spectral analyzer (OSA) to characterize the output from the FOPO. The OSA allows us to plot the output spectrum for different central wavelengths and pump powers. In the measurements of Stokes peak versus the power of the pump beam we use a power meter placed after the SPD. The wavelength is tuned by shifting the position and orientation of M_4. The result is that the Stokes moves away or towards to the pump center wavelength depending upon the alignment. Our procedures consist to measuring the output spectrum and average power for different pump powers and output wavelengths.

Our second harmonic generation Frequency Resolved Optical Gating (SHG-FROG) apparatus is a Michelson interferometer with offset beams coupled through a beta-BaB2O4 (BBO crystal) in order to obtain background-free SHG. The output from the FOPO is coupled to the SHG-FROG with the help of gold mirrors as seen in the schematic on figure 4.2 . In this manner, two photons carrying the same amount of energy are reflected from a beam splitter, when completed aligned, into a BBO crystal, which by using its $\chi^{(2)}$ linearity, will produce a photon carrying the twice the energy of one incident photon as seen in figure 4.3.

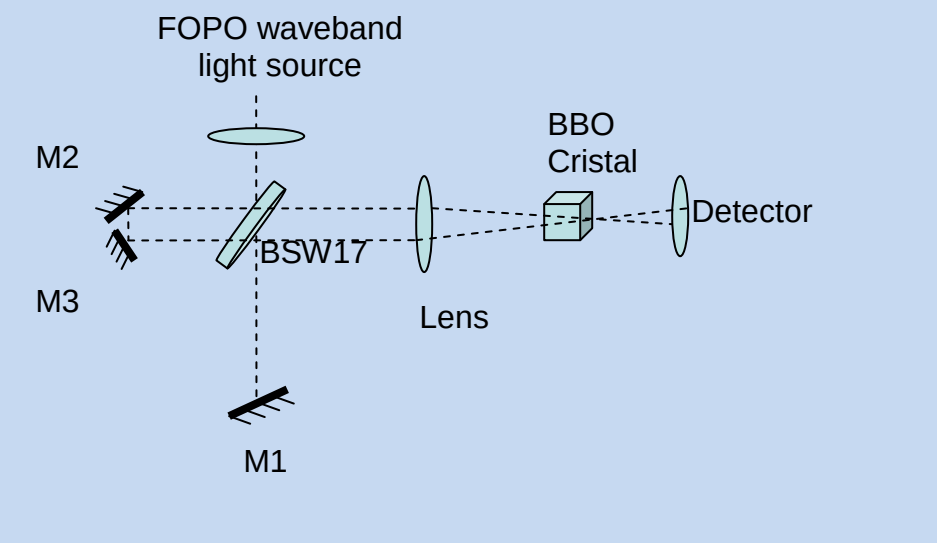

Figure 4.2 The schematic of the frequency resolved optical gating, (FROG) apparatus used in the experiment in order to determinate the temporal and spectral amplitude and phase of the FOPO output pulses.

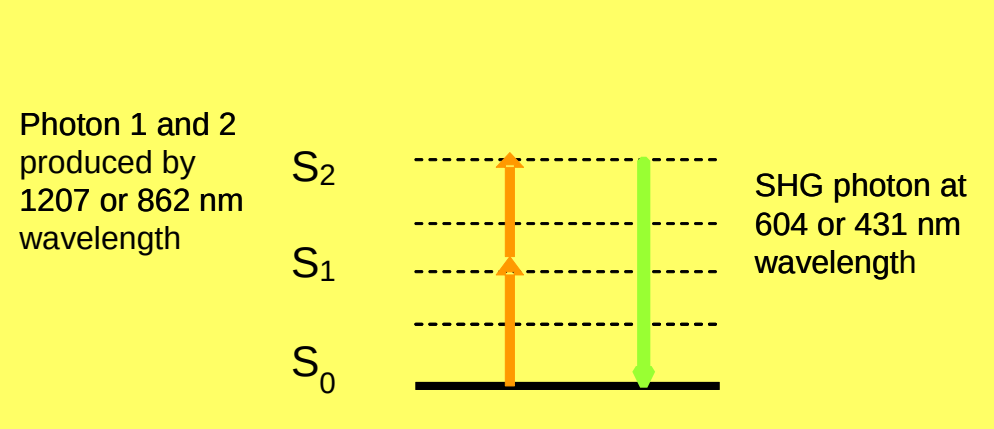

Figure 4.3 the virtual energy diagram depicting a second harmonic generation process, which occurs in the FROG apparatus described above. Two photons carrying equal amount amount of energy are combined and a photon with energy equal to the two photons combine combined and twice the frequency is generated.

The SHG output is coupled using 2-inch focal length lens into an optical spectrum analyzer (OceanOptics, HR2000+) via a multimode fiber. The scanning arm of the interferometer is actuated with a motion controlled translation stage (Newport, Inc., MFA-CC). LabView software acquires the spectrogram (a 2-dimensional map of spectrum as a function of delay) and controls the entire experiment. Analysis of the spectrogram including phase retrieval, is performed using commercially available software (FemtoSoft Technologies v3.2.2). This technique permits the determination of the temporal and spectral amplitude and phase of the pulses under test.

Results

Figure 4.4 shows optical spectra recorded at the output of the FOPO. From this plot one observes that the system is operating over a wavelength range of about 1200 nm up to 1350 nm. The output power varies 50% between the maximum power at ~1270 nm and the minimum power at ~ 1220 nm. The system is tunable over 150 nm overall. The pulse quality observed in this system FROG apparatus reveals uniform pulse shapes with the duration varying from 105 to 118 fs.

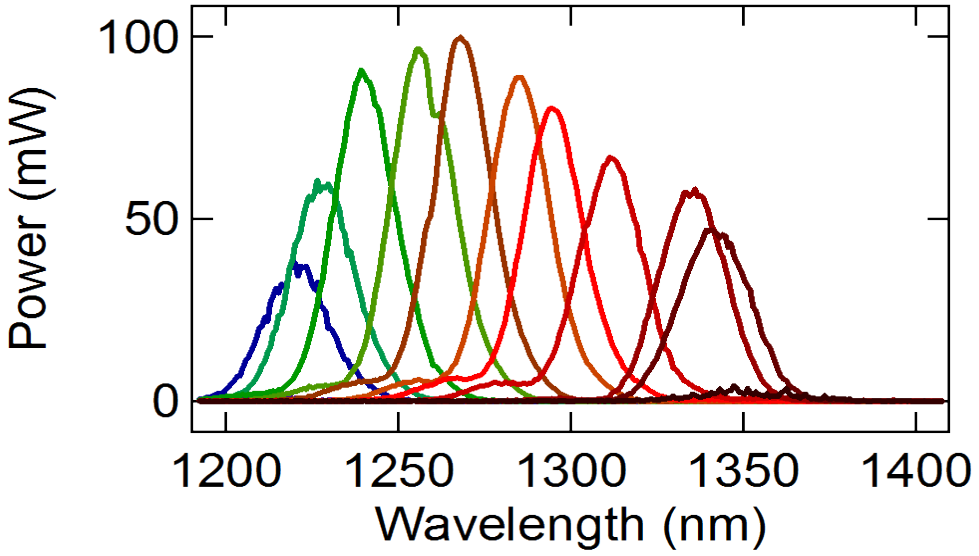

Fig 4.4 A composite of optical spectra recorded as the cavity length of the FOPO is varied. The FOPO depicted here is pumped by a mode-locked 50-MHz mode-locked Ytterbium-doped fiber laser (PolarOnyx - Uranus). In the spectrum the power varies across the range of wavelength tunability, where the maximum power of ~ 100 mW is at ~1270 nm.

The plot of amplitude and phase versus time shown in figure 4.5 presents a quadratic change at the center of the pulse, for short output wavelengths in the phase in respect to time. However, in the case of long output wavelengths the phase varies cubically, but at the center of the pulse the phase is relatively constant. The amplitude here in both cases is normalized to 1.0 at logarithmic scale. The intensity, or amplitude of the FOPO output is measured using a power detector to be 50mW and 70 mW for the short and long wavelengths outputs respectively. The output center wavelength is 862 nm and 1207 nm measured by the OSA program connected to the SHG-FROG apparatus.

Performance of idler FOPO output

- 1207 nm (when quadrupled 302 nm)
- 118 fs (FWHM)
- Power at 70 mW

SHG FROG trace

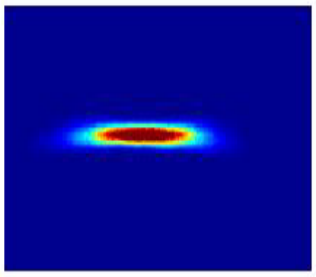

Temporal amplitude (markers/left) phase (line/right)

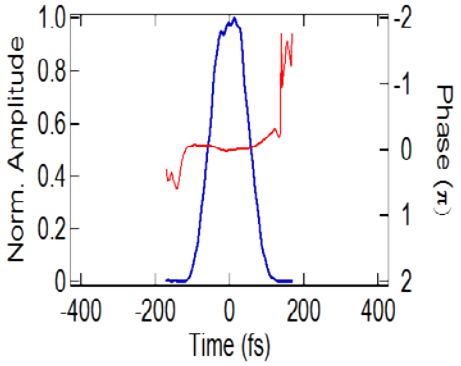

Performance of FOPO analyzed by SHG-FROG:

- 862 nm (when 287 nm tripled)
- 105 fs pulses produced by FWHM
- System power output Power 50 mW

SHG FROG trace

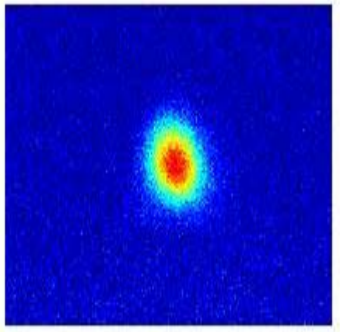

Temporal amplitude (markers/left) phase (line/right)

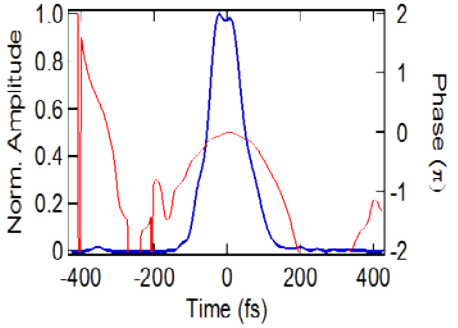

Figure 4.5 In this figure an image of a short and long wavelength FOPO output is shown. The pulse is viewed from the top. The plot of amplitude and phase versus time is also shown, where pulse duration and phase variation is given.

Discussion

The system used in this experiment is capable of producing a FOPO output that is tunable in terms of wavelength. The broad tunability of this system is due to the short PCF that can be employed in this case. As in the previous system described in this study, the length of the PCF is determined by the temporal width of the laser pump pulses, the pump repetition rate, and the fiber parameters, which can promote phase matching. The pulse duration of 300 fs produced by the pump used in this experiment permitted us to use a short, 3 cm, PCF that facilitates wavelength tunability by increasing the range of conditions that phase matching can be obtained without compromising the gain necessary for the system to oscillate.

The shape and temporal width of the output demonstrated through the results, shown in figure 4.5, obtained by the FROG apparatus, show us that the pulses are short and applicable for the applications in aim. The shape of the output pulses is indicative of the optimum length for the Fabry-Perot cavity.

The poor stability of this system is due to several factors that are related to its configuration and laser pump used. The beam in this system is maintained at a higher position than in the configuration adopted on the previous system. Moreover, due to

the fact that a short PCF is used, the Fabry-Perot cavity is larger and more mirrors have to be used increasing the loss, reducing the gain, and increasing the chance of misalignment in the system. We also infer that the laser pump contributes somewhat to the lack of stability of this system compared to the other system because the Ytterbium-doped fiber (PolarOnyx - Uranus) laser is a novel technology relatively new in the market. In spite of the smaller stability of this system, the tunability range of a 150 nm and short pulse duration less than 120 fs pulses enable us to employ this system on the envisioned applications (Goulart-Pailo, 2009).

Conclusions

The system described in this study is tunable over 150 nm in the near infrared. This wavelength tunability range is fundamental for the envisioned application for cellular imaging processes. We observe pulse durations as short as 130 fs and output powers approaching 100 mW average (12 kW peak). However, the system is less stable and reliable when compared to the previous system described in this study, which limits the system's performance during extended periods of time. Moreover, detailed studies of the pulse quality reveal, that nearly transform-limited 130 fs pulses can be generated,

but the pulse quality becomes asymmetric and chirped when tuned away from the optimal setting. This feature can interfere with the synchronization of the FOPO's output when applied to imaging techniques such as CARS. Pulse quality is also dependent on the pump power relative to the threshold for oscillation where there is a small dynamic range of powers (~10% of the threshold value) over which optimal pulses are generated. In spite of these, this system embodies the necessary characteristics for cellular imaging acquisition because it offers a wide range of wavelength tunability between FOPO's output spectral bands and reasonable power.

Chapter V

Perspectives:

Possible Applications of FOPO for Cellular Imaging Settings

Introduction

Nonlinear optical (NLO) microscopy refers to a set of techniques used to generate chemically selective images of non-stained biological samples (Chen, 2010; Cheng, 2008). Selective imaging associated with functionality, health, or structure within a tissue can be performed (Kano, 2005). The techniques are powerful, but generally require multiple, synchronously-pulsed lasers whose wavelengths can be freely adjusted (Ganikhanov, 2006). In this study we describe applications of the developed FOPO to multimodal nonlinear optical microscopy as a proof of concept. We used the FOPO system described in chapter four of this thesis to excite C-D and C=C bonds. The motivation of this study is to apply the femtosecond/ short fiber OPO tested in this investigation to serve as an efficient and versatile laser light source to Multimodal NLO microscopy.

We hypothesize that the femtosecond/short fiber OPO described in this investigation operates via the nonlinear optical response of optical fibers, produces a range of wavelengths analogous to the bonds of interest, C-D and C=C bonds we wish to measured

Methods

In this experiment, as seen in the schematic presented in Figure 5.1, the output of the FOPO at 850 nm, is coupled together with a 1032 nm laser pump center wavelength into a nonlinear optical microscopy setup (Pegoraro, 2009; Wise, 2009). Diverse NLO microscopic images, shown in Figures 5.2 and 5.3 were produced as a proof of concept of the feasibility of the FOPO into cellular imaging settings. One of the bond of interest is a C-D bond present on of 3T3-L1 cells cultured with 50 μm of deuterated palmitic acids as seen in Figure. 5.2. We recorded images of lipid droplets inside of the cells, which are clearly visible in the CARS images (Chen, 2010).

The FOPO system, in this case, is tuned to 850 nm in order to excite the C-D stretching modes at 2100 cm^{-1}. A typical transmission image and the corresponding CARS image are shown in Figure 5.2a and 5.2b, respectively. To verify that the signal is truly from CARS, we perform the same measurement with the pump (1032 nm wavelength) and Stokes (850 nm wavelength) beams separated in time which leads to the dark image in Figure 5.2c. Confocal Raman microspectroscopic analysis of the lipid droplets using the same microscope reveal a

distinctive peak near 2100 cm^{-1} corresponding to the C-D stretching vibration as seen in Figure 5.2d.

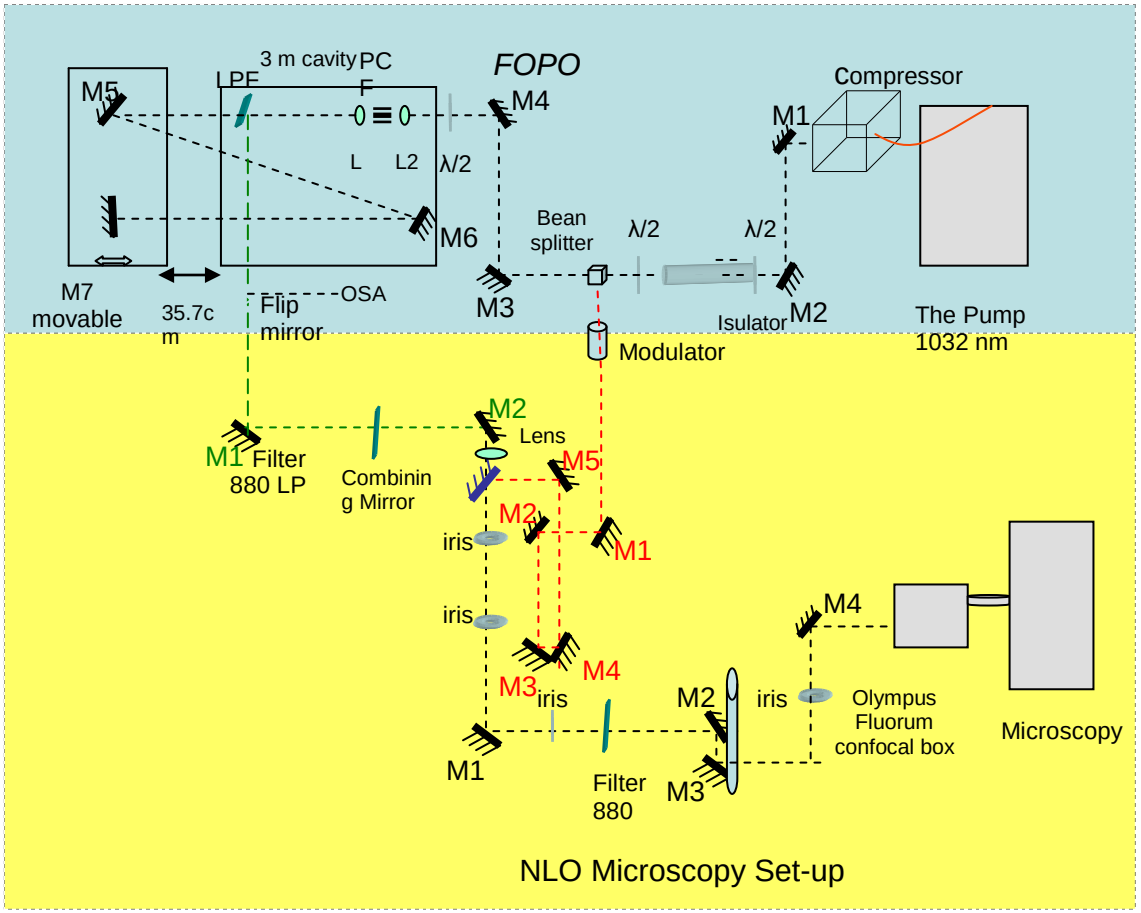

Fig 5.1 Schematic of FOPO pumped by a fs Ytterbium doped fiber laser (Polaronix-Uranius) used as a laser source, enclosed in blue, for NLO microscopic setup enclosed in yellow.

We further demonstrated CARS-based multimodal imaging of a rat spinal cord white matter using the same FOPO system. The output wavelength in this case was tuned to 880 nm to excite C=C vibrations at 1650 $cm.^{-1}$ The tissue sample was fixed and the axons were immuno-labeled with NF160. The forward-detected CARS image in Figure 5.3a shows parallel aligned myelin fibers. The TPEF image of the labeled axons shown in Figure 5.3b was obtained simultaneously. The overlaid image in Figure 5.3c and the magnified area in Figure 5.3d show the relative position of myelin sheaths and axons.

Therefore, we use the energy difference between the FOPO output and the laser pump center wavelength, 850 nm wavelength and 1032 nm wavelength, corresponding to 2100 cm^{-1} wave number and 1650 cm^{-1} in order to excite the C-D and C=C bonds of interest.

Samples Preparation

De Novo Lipid Synthesis in 3T3-L1 Cells. De novo lipid synthesis was induced using an adipogenesis assay kit (catalog no. ECM 950, Chemicon International). 3T3-L1 cells were grown to confluence in Dulbecco's Modified Eagle's Medium (DMEM) consisting of 25 mM of glucose supplemented with 10% calf serum and penicillin/streptomycin. On day 0, the cells were

induced with the initiation medium composed of 0.5 mM isobutylmethylxanthine (IBMX) and 1 μM dexamethasone in DMEM supplemented with 10% fetal calf serum and penicillin (100 units/mL)/streptomycin (100 μg/mL). On day 2, the initiation medium was replaced with the progression medium composed of 10 μg/mL insulin in DMEM supplemented with 10% fetal calf serum and penicillin/streptomycin. On day 4, the progression medium was replaced with the maintenance medium (DMEM supplemented with 10% fetal calf serum and penicillin/streptomycin). From day 4 to day 14, the cells were kept in maintenance medium with new maintenance medium being replaced every two days. Cells were incubated at 37 °C with 5% CO2. (Slipchenko, 2009**)**

Rat Spinal Cord Preparation: In order to separate the ventral white matter from the gray matter of a rat spinal cord a saggital the spinal cord was first split into two halves and then cut radially. In a chambered glass cover slip the isolated ventral white matter strip was mounted on a and it was kept in oxygen bubbled Krebs' solution (NaCl 124 mM, KCl 2 mM, KH2PO4 1.2 mM, MgSO4 1.3 mM, CaCl2 2 mM, dextrose 10 mM, NaHCO3 26 mM, and sodium ascorbate 10 mM, equilibrated with 95% O2, 5% CO2). The samples for CARS imaging of axonal myelin were not labeled. The samples for simultaneous CARS imaging of axonal

myelin and TPEF imaging of Ca21 were incubated in a Ca21 free Krebs' solution that contained 40 mM Oregon green 488 (BAPTA-2, Molecular Probes, Eugene, OR) for 2 h and then washed with normal Krebs' solution (containing 2 mM Ca21) before imaging. The axons in the sample maintained good morphology for at least 10 h in the chamber. Dioleoyl phosphatidylcholine (DOPC) and dipalmitoyl phosphatidylcholine (DPPC), and cholesterol were purchased from Avanti Polar Lipids (Alabaster, AL) and used without further purification. (Wang, 2005)

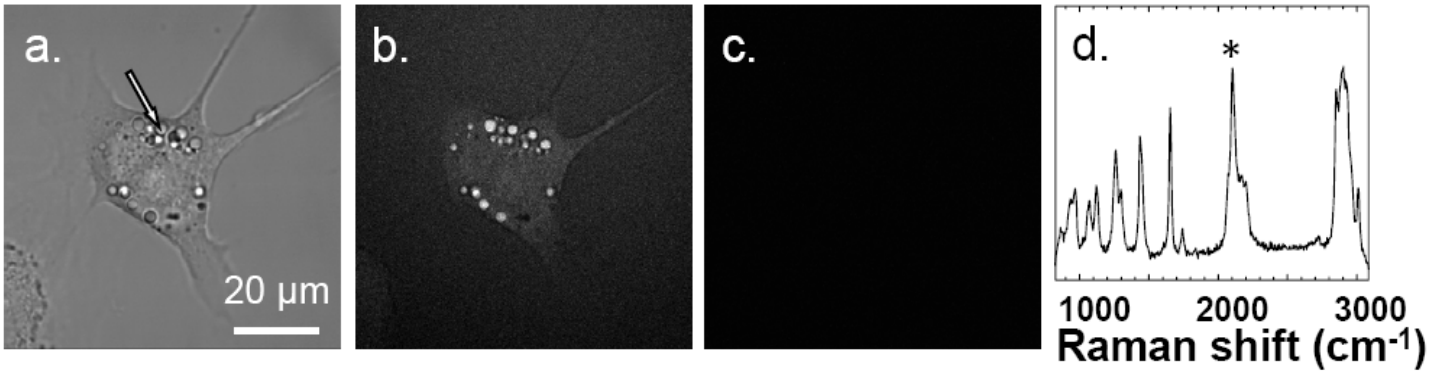

Fig. 5.3. Imaging C-D bonds in 3T3-L1 cells with FOPO-based CARS. (a) Transmission image. (b) Forward detected CARS image at $\omega_1 - \omega_2 = 2074$ cm^{-1}. (c) CARS Image with asynchronous pump and Stokes beams. (d) Raman spectrum obtained at the point indicated by the arrow in (a). C-D stretch is indicated by asterisk. The average laser pump (1032 nm) and Stokes (850 nm) powers were 4 mW and 25 mW at the sample position, respectively. The total uptaken imaging time per pixel was 20 μs.

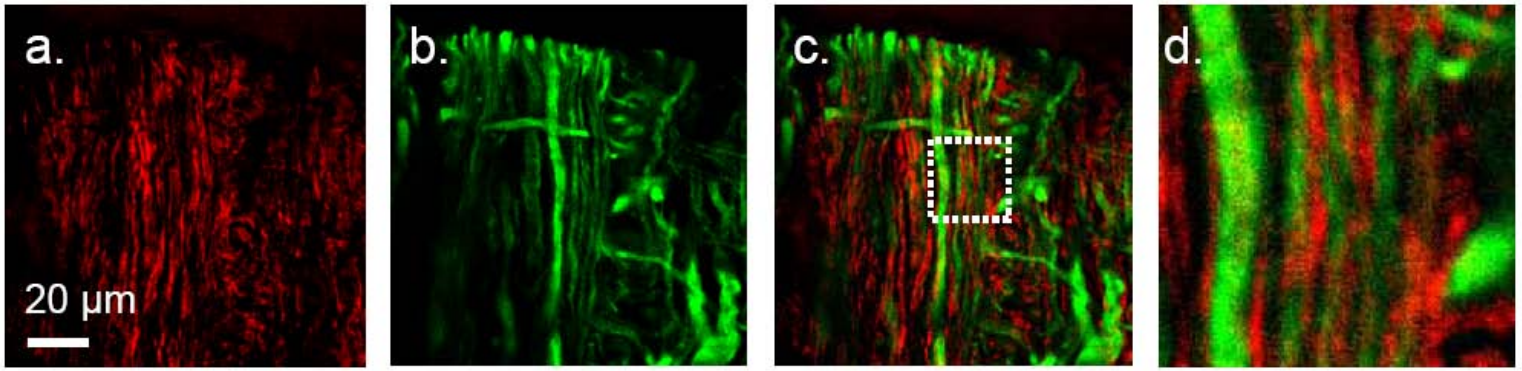

Fig. 5.4. The multimodal images of rat spinal cord. (a) Forward detected CARS image of myelin sheath at $\omega_1 - \omega_2 =$ 1673 cm^{-1}. (b) TPEF image of axons labeled with NF160. (c) Overlaid CARS and TPEF images. (d) Magnified segment of the overlaid images. The average laser pump (1032 nm) and Stokes (850 nm) powers were 3.3 mW and 15 mW at the sample position, respectively.

General Conclusions

In summary, we have performed the first demonstration of the multimodal CARS microscopy using a fiber laser and a FOPO. In our experiment, the FOPO generates up to 25 mW output that is tunable between 840 nm and 930 nm. In combination with the fiber laser, high-speed, high-quality CARS and TPEF imaging were realized. The current system allows one to probe vibrational transitions between 1050 cm^{-1} and 2220 cm^{-1}. Further development is under way to improve the performance in terms of the wavelength tuning range, stability and the output power. It was shown that by using modified PCFs, the output as high as 100 mW is attainable. Another challenge is that the FOPO output has a broad spectrum in comparison with the laser pump spectrum , limiting CARS efficiency. One approach to narrow the FOPO output is to introduce extra dispersive elements within the FOPO cavity. Finally, an all-fiber OPO cavity pumped by fiber laser needs to be developed to ultimately eliminate the free space design, thus providing a truly compact, stable laser source for coherent Raman microscopy (Pegoraro, 2009).

References

1. Agrawal, G. (2000). *Nonlinear fiber optics* Springer. 2nd Ed. Academic Press, San Diego, CA, 2001.

2. Agrawal, G. (2000). *Nonlinear fiber optics* Springer. 4nd Ed. Academic Press, San Diego, CA, 2007

3. Boron, W. F., & Boulpaep, E. L. (2003). *Medical physiology : A cellular and molecular approach*. Philadelphia, PA: W.B. Saunders. Retrieved from /z-wcorg/

4. Chen, B., Sung, J., & Lim, S. -. (2010). Frequency modulation coherent anti-Stokes Raman scattering (FM-CARS) microscopy based on spectral focusing of chirped laser pulses*., 7569* Retrieved from SCOPUS database.

5. Cheng, J. -. (2008). Coherent anti-Stokes Raman scattering microscopy. Focal Point, 61(9).Retrieved from SCOPUS database.

6. Cheung, E. C., & Liu, J. M. (1990). Theory of a synchronously pumped optical parametric oscillator in steady-state operation. *J.Opt.Soc.Am.B, 7*(8), 1385-1401. Retrieved from SCOPUS database.
7. Ebrahimzadeh, M. (2003). Mid-infrared ultrafast and continuous-wave optical parametric oscillators. *Solid-State Mid-Infrared Laser Sources, Topics in applied physics, 89*, 179-218. Retrieved from SCOPUS database.

8. Eriksson, E., & Reish, R. G. (2008). Scars: A review of emerging and currently available therapies. *Plastic and Reconstructive Surgery, 122*(4), 1068-78.

9. Evans, C. L., Potma, E. O., Puoris'haag, M., Côté, D., Lin, C. P., & Xie, X. S. (2005). Chemical imaging of tissue in vivo with video-rate coherent anti-Strokes Raman scattering microscopy. *Proceedings of the National Academy of Sciences of the United States of America, 102*(46), 16807-16812. Retrieved from SCOPUS database.

10. Freudiger, C. W., Min, W., Saar, B. G., Lu, S., Holtom, G. R., He, C., et al. (2008). Label-free biomedical imaging with high sensitivity by stimulated Raman scattering microscopy. *Science, 322*(5909), 1857-1861. Retrieved from SCOPUS database.

11. Ganikhanov, F., Carrasco, S., Xie, X. S., Katz, M., Seitz, W., & Kopf, D. (2006). Broadly tunable dual-wavelength light source for coherent anti-Stokes Raman scattering microscopy. *Optics Letters, 31*(9), 1292-1294. Retrieved from SCOPUS database.

12. Goulart-Pailo, C., Gu, C., & Sharping, J. E. (2009). Full characterization of femtosecond pulses at 1225-1350 nm produced by a high power fiber optical parametric oscillator. *Conference on Lasers and ElectroOptics/International Quantum Electronics Conference,* Retrieved from SCOPUS database.

13. Hecht,Eugene.Hansryd, J., Adrekson P.A. (2002). Fiber Based Parametric Amplifiers and Their Applications. *IEE Journal, 8(3)*. Retrieved from SCOPUS database.

14. Hecht,Eugene. (1998) *Optics. Hecht*. Addison-Wesley; Reading, Mass. 1998.

15. Kano, H., & Hamaguchi, H. -. (2005). Ultrabroadband (>2500 cm-1) multiplex coherent anti-Stokes Raman scattering microspectroscopy using a supercontinuum generated from a photonic crystal fiber. *Applied Physics Letters, 86*(12), 1-3. Retrieved from SCOPUS database.

16. Keller, U. (2003). Recent developments in compact ultrafast lasers. *Nature, 424*(6950), 831-838. Retrieved from SCOPUS database.

17. Kieu, K., Saar, B. G., Holtom, G. R., Sunney Xie, X., & Wise, F. W. (2009). High-power picosecond fiber source for coherent Raman microscopy. *Optics Letters, 34*(13), 2051-2053. Retrieved from SCOPUS database.

18. Krauss, G., Hanke, T., Sell, A., Träutlein, D., Leitenstorfer, A., Selm, R., et al. (2009). Compact coherent anti-Sokes Raman scattering microscope based on a picosecond two-color er:Fiber laser system. *Optics Letters, 34*(18), 2847-2849. Retrieved from SCOPUS database.

19. Le, T. T., Duren, H. M., Slipchenko, M. N., Hu, C. D., & Cheng, J. X. (2010). Label-free quantitative analysis of lipid metabolism in living caenorhabditis elegans. *Journal of Lipid Research, 51*(3), 672-677. Retrieved from SCOPUS database.

20. Marhic, M. E. (2007). *Fiber Optical Parametric Amplifiers, Oscillators and Related Devices,* Retrieved from SCOPUS database.

21. Moore, J. H. D., Davis C. C., Coplan M. A. (2003). *Building Scientific Apparatus: A Practical Guide Design and Construction*. 247-273. 3nd Ed. Westview Press. Boulder , CO.

22. Murugkar, S., Evans, C. L., Xie, X. S., & Anis, H. (2009). Chemically specific imaging of cryptosporidium oocysts using coherent anti-Stokes Raman scattering (CARS) microscopy. *Journal of Microscopy, 233*(2), 244-250. Retrieved from SCOPUS database.

23. NKT Photonics, (2009) "Supercontinuum generation in Photonic Crystal Fibers" 2 www.NKTPhotonics.com.

24. Pegoraro, A. F., Ridsdale, A., Moffatt, D. J., Pezacki, J. P., & Stolow, A. (2009). High performance multimodal CARS microscopy using a single femtosecond source*., Optics Express 17, 2984-2996.* Retrieved from SCOPUS database.

25. Pegoraro, A. F., Ridsdale, A., Moffatt, D. J., Pezacki, J. P., Thomas, B. K., Fu, L., et al. (2009). All-fiber CARS microscopy of live cells. *Optics Express, 17*(23), 20700-20706. Retrieved from SCOPUS database.

26. Sharping, J. E. (2008). Microstructure fiber based optical parametric oscillators. *Journal of Lightwave Technology, 26*(14), 2184-2191. Retrieved from SCOPUS database.

27. Sharping, J. E., Fiorentino, M., Kumar, P., & Windeler, R. S. (2002). A microstructure-fiber based optical parametric oscillator. Opt. lett.27. Retrieved from 1675 Retrieved from SCOPUS database.

28. Sharping, J. E., Fiorentino, M., Kumar, P., & Windeler, R. S. (2002). Optical parametric oscillator based on four-wave mixing in microstructure fiber. *Optics Letters, 27*(19), 1675-1677. Retrieved from SCOPUS database.

29. Sharping, J. E., Pailo, C., Gu, C., Kiani, L., & Sanborn, J. R. (2010). Microstructure fiber optical parametric oscillator with femtosecond output in the 1200 to 1350 nm wavelength range. *Optics Express, 18*(4), 3911-3916. Retrieved from SCOPUS database.

30. Silberberg, Y. (2009). Quantum coherent control for nonlinear spectroscopy and microscopy. Annu. Rev. of Chem. 60 9(277-292). Retrieved from SCOPUS database.

31. Slipchenko M. N., Le T. T., Cheng H., Cheng J. (2009). High-Speed vibrational Imaging and Spectral Analysis of Lipid Bodies by Compund Raman Microscopy. J. Phys. Chem. B, 113, 7681-7686. Retrieved from SCOPUS database.

32. Spence, D. E., Kean, P. N., & Sibbett, W. (1991). 60-fsec pulse generation from a self-mode-locked ti:Sapphire laser. *Opt.Lett., 16*(1), 42-44. Retrieved from SCOPUS database.

33. Tong, L., Cobley, C. M., Chen, J., Xia, Y., & Cheng, J. -. (2010). Bright three-photon luminescence from gold/silver

alloyed nanostructures for bioimaging with negligible photothermal toxicity. *Angewandte Chemie - International Edition, 49*(20), 3485-3488. Retrieved from SCOPUS database.

34. Verdeyen, J. F. (1994). *Laser Electronics*. 3nd Ed. Prentice Hall, London, Great Britain.

35. Wang, H., Fu, Y., Huff, T. B., Le, T. T., Wang, H., & Cheng, J. -. (2009). Chasing lipids in health and diseases by coherent anti-stokes raman scattering microscopy. *Vibrational Spectroscopy, 50*(1), 160-167. Retrieved from SCOPUS database.

36. Wang, H., Fu, Y., Zickmund, P., Shi R., Cheng, J. -. (2005). Coherent Anti-Stokes Raman Scattering Imaging of Axonal Myelin in Live Tissues. *Biophysical Journal 89*(1), 581-591. Retrieved from SCOPUS database.

37. Wise, F. W., Kieu, K., Saar, B., Holtom, G., & Xie, S. (2009). Fiber lasers for CARS microscopy. *7183* Retrieved from SCOPUS database.

38. Wong, G. K. L., Murdoch, S. G., Leonhardt, R., Harvey, J. D., & Marie, V. (2007). High-conversion-efficiency widely-tunable all-fiber optical parametric oscillator. *Optics Express, 15*(6), 2947-2952. Retrieved from SCOPUS database.

39. Xu, Y. Q., Murdoch, S. G., Leonhardt, R., & Harvey, J. D. (2009). Raman-assisted continuous-wave tunable all-fiber optical parametric oscillator. *Journal of the Optical Society of America B: Optical Physics, 26*(7), 1351-1356. Retrieved from SCOPUS database.

40. Zhou, Y., Cheung, K. K. Y., Yang, S., Chui, P. C., & Wong, K. K. Y. (2009). A time-dispersion-tuned picosecond fiber-optical parametric oscillator. *IEEE Photonics Technology Letters, 21*(17), 1223-1225. Retrieved from SCOPUS database.

Appendix 3: Qualifier exam proposal of Chenji Gu

Photonic Crystal Fiber Based Ultrashort Pulses: Generation, Propagation and Characterization

Submitted by Chenji Gu

PI: Prof. Jay E. Sharping

School of Natural Sciences

University of California, Merced

Merced, CA 95344

cgu2@ucmerced.edu

ABSTRACT

Photonic Crystal fibers give us numerous outstanding optical properties, such as endless single mode, high nonlinearity and controllable chromatic dispersion. It is possible to make optical devices based on these different functional fibers. One can make light sources which are compact, portable, widely tunable, ultrashort pulse duration, and which deliver high peak powers. Particularly, our research focus is on fiber based optical parametric oscillators, and we generate tsub-100 fs tunable IR output. The detailed characterization of output pulses by the technology called, Frequency Resolved Optical Gating, shows that the pulse shape of output could be either well behaved or very complex depending on the changes the degree of synchronization. We simulate pulse propagation within fibers as well as model the fiber based optical parametric amplifiers. The theory suggests that it is possible to have a self-similar pulse based on our current fiber based optical parametric oscillators. Furthermore, based on the understanding above, we are working on improving the quality of pulsed output both theoretically and experimentally. An easy approach is to use a fiber based parametric amplifier to let the pulse evolve into self-similar region, and have another optional fiber for pulse compression.

1. INTRODUCTION AND MOTIVATION

In the work proposed here we aim to have a greater understanding of pulse generation and evolution in photonic crystal fibers. We aim to apply new understanding in building pulsed light sources addressing needs in pulsed-light microscopy and spectroscopy.

1.1 Introduction of Photonic Crystal fibers

Pioneered by Prof. Philip St. J. Russell's research group in the 1990s, Photonic-crystal fibers (PCFs) are a new class of optical fibers, which give unique confinement characteristics not possible in conventional optical fibers. PCF is now finding applications in fiber-optic communications, fiber lasers, nonlinear devices, high-power transmission, highly sensitive gas sensors, and other areas [1].

This class of fiber is referred to by other names like holey fiber, hole-assisted fiber, microstructure fiber, or microstructured fiber. Control over the geometrical design of the fiber leads to control over its waveguide properties. One can spatially vary an arrangement of very tiny and closely spaced air holes which go through the whole length of fiber. Such air holes can be obtained by using a preform with holes, made by stacking capillary tubes (stacked tube technique). Soft glasses and polymers also allow the fabrication of preforms for photonic crystal fibers by extrusion. There is a great variety of hole arrangements, as shown in Fig. 1 [1], leading to PCFs with very different properties.

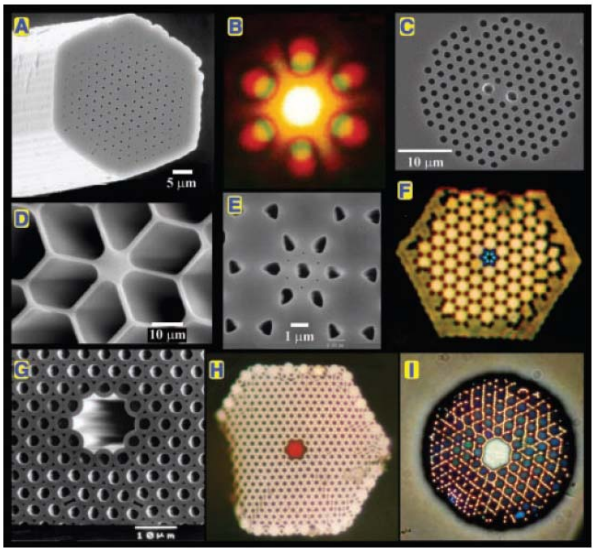

Fig. 1 Images from [1] show an assortment of optical (OM) and scanning electron (SEM) micrographs of PCF structures. (A) SEM of an endlessly single-mode solid core PCF. (B) Far-field optical pattern produced by (A). (C) SEM of a recent birefringent PCF. (D) SEM of a small (800 nm) core PCF. (E) SEM of the first photonic band gap PCF. (F) Near-field OM of the six-leaved blue mode. (G) SEM of a hollow-core photonic band gap fiber. (H) Near-field OM of a red mode in hollow-core PCF. (I) OM of a hollow-core PCF.

Owing to different designs of the hole pattern (concerning the basic geometry of the lattice, the relative size of the holes, and possibly small displacements), one can have interesting optical properties, strongly dependent on the design details:

- It is possible to obtain a high numerical aperture of 0.7 of multimode fibers [2].
- Single-mode guidance over wide wavelength regions (endlessly single-mode fiber) is obtained for small ratios of hole size and hole spacing [3].
- Extremely small or extremely large mode areas are possible. These lead to strong or weak optical nonlinearities. PCFs can be made with a low sensitivity to bend losses even for large mode areas [4, 9].
- Certain hole arrangements result in a photonic bandgap, where guidance is possible even in a hollow core, as a higher refractive index in the inner part is no longer required. Such air-guiding hollow-core fibers are interesting e.g. for dispersive pulse compression at high pulse energy levels.
- Particularly for larger holes, there is the possibility to fill gases or liquids into the holes. This can be exploited for fiber-optic sensors, or for variable power attenuators.
- Asymmetric hole patterns can lead to extremely strong birefringence for polarization-maintaining fibers [8] as well as polarization-dependent fibers [5，6].
- Unusual chromatic dispersion properties, especially anomalous dispersion in the visible wavelength region [8].

In summary, there are substantial design freedoms, allowing for different combinations of desirable

parameters of PCFs.

1.2 Motivation for PCFs based devices

Solid-state laser systems often use $\chi^{(2)}$ crystals for stable generation of wavelength-agile short pulsed laser radiation [12]. One can have synchronous short pulses trains at different wavelengths, and the wavelength can be widely tunable at certain frequency domain. These pulse trains are useful in pump-probe measurements such as probing the carrier lifetimes in semiconductors and spectroscopically resolving fast chemical and biological reactions [13- 15]. Although commercial solid-state laser systems are quite successful and commonly used, they are still kind of expensive. During these years, facilitated by the development of PCFs there is a trend towards using ultrafast fiber lasers. The major drawbacks of fiber lasers are their limited tunable wavelength and pulse duration. Fiber-based optical parametric oscillators, operating through four-wave mixing (FWM) mediated by the $\chi^{(3)}$ nonlinearity of glass, promise to address this shortcoming. The advantages comparing to crystals based $\chi^{(2)}$ are [24]:

- The FWM phase-matching bandwidth can be continuous and hundreds of nanometers wide.
- The signal gain occurs at wavelengths near to, as well as far from, that of the pump.
- The transverse mode quality of fiber-based oscillators is exceptionally good.
- A fiber-based gain medium lends itself to further integration with fiber components.
- The widespread adoption of ultrafast systems will be greatly facilitated by the development of fiber-integrated wavelength-agile synchronous sources.

So one of our motivations is to satisfy the need for compact tunable pulsed light sources. On the other hand, the comparison in Fig. 2 shows the importance of managing pulse duration and shape, so there is also a need to theoretically understand the pulse evolution as a platform for applied mathematics. Usually this is a job for numerical solutions of the nonlinear Schrödinger equation (NLSE) [10], which will be discussed in later sections. Furthermore, on the experimental side we need to fully characterize ultrashort pulses, which is impossible for any fast detector. So we need to have some other more powerful measurement, such as Frequency Resolved Optical Gating (FROG) which will be discussed in chapter 3.

1.3 Pulse propagation within fibers

Since PCFs have so many unusual optical properties, it is important know the evolution of optical pulses during the propagation within the fibers. Usually pulse propagation problems can be modeled as generalized NLSE [10]:

$$\begin{aligned}\frac{\partial A(t,z)}{\partial z} &= -\beta_1 \frac{\partial A(t,z)}{\partial t} - \frac{i\beta_2}{2}\frac{\partial^2 A(t,z)}{\partial t^2} + \frac{\beta_3}{6}\frac{\partial^3 A(t,z)}{\partial t^3} - \frac{\alpha}{2}A(t,z) \\ &+ i\gamma\left[\left|A(t,z)\right|^2 A(t,z) + \frac{i}{\omega_0}\frac{\partial\left(\left|A\right|^2 A\right)}{\partial t} - T_R\frac{\partial\left(\left|A\right|^2\right)}{\partial t}A\right]\end{aligned} \tag{1}$$

where α is the fiber loss (in inverse meters 1/m), γ is the fiber nonlinearity (in inverse Watt meters

$(Wm)^{-1}$), β_2 is the fiber's second-order dispersion (in seconds squared per meter (s^2/m), β_3 is the fiber's third-order dispersion (in seconds cubed per meter (s^3/m), T_R provides an approximate way of incorporating the Raman response.

For example, consider the problem of pulse propagation in a fiber amplifier. Two sets of parameters are available for comparison [11]: (a) Normal dispersion, β_2 =+25 $ps^2\,km^{-1}$, γ =5 $W^{-1}\,km^{-1}$, g =1.92 m^{-1} and (b) anomalous dispersion, β_2 =-25 $ps^2\,km^{-1}$, γ =5 $W^{-1}\,km^{-1}$, g =1.54 m^{-1}. The input pulse has a hyperbolic secant profile, Temporal FWHM is 300 fs, and 12-pJ energy.

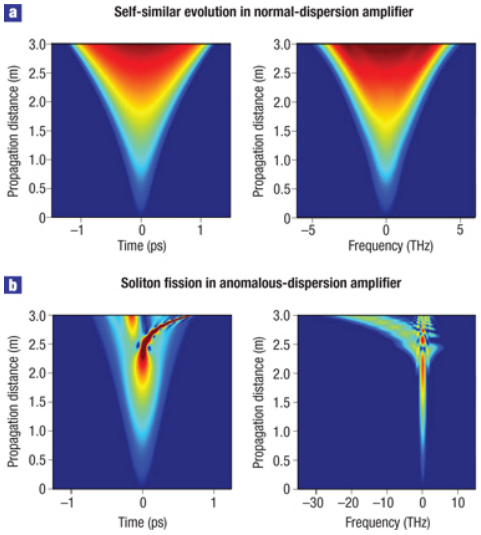

Fig. 2 Images from [11] simulation of pulse evolution in fiber amplifiers comparing self-similar evolution with soliton fission. Normal (a) and anomalous (b) dispersion using parameters typical of Yb- and Er-doped gain media respectively. The figures are false-colour representations (on a logarithmic scale) of the pulse temporal intensity and power spectrum.

The comparison in Fig. 2 clearly shows the difference between amplification with normal and anomalous dispersion. With normal dispersion we obtain self-similar dynamics. Amplification is associated with the simultaneous increase in both temporal and spectral widths and the absence of any wave breaking or pulse distortion. In contrast, for an amplifier with the same gain yet with anomalous dispersion, as the pulse energy increases with amplification, instabilities become apparent and the pulse breaks up owing to the effect of soliton fission. In this case, both the pulse temporal and spectral structure is complex and the output characteristics would be undesirable for many applications.

2. PCF Based Optical Parametric Amplifiers And Oscillators

2.1 Experimental setup of fiber optical parametric oscillators

Two configurations are illustrated schematically in Fig. 3. A fiber optical parametric amplifier (FOPA) (Fig. 3 (a)) includes both "pump" and "signal" fields at the input where the system has been designed such that energy is shifted from the strong pump to the weaker signal resulting in amplification of the signal. Energy conservation dictates the generation of a third "conjugate" (often called the idler) field

whose frequency is such that $2\omega_0 = \omega_1 + \omega_2$, where ω_0, ω_1, ω_2 are the angular frequencies of the pump, signal, and conjugate fields, respectively. The generation of the conjugate field means that the parametric amplifier configuration can also be used for wavelength conversion. The second configuration (Fig. 3(b)) is device where a single "pump" field of sufficient power is launched into one end of the fiber, but the presence of a cavity allows for the coherent buildup of the ASE in a manner similar to laser action. Figure 3(c) illustrates the four-photon process and energy conservation within fiber optical parametric amplifier or oscillator.

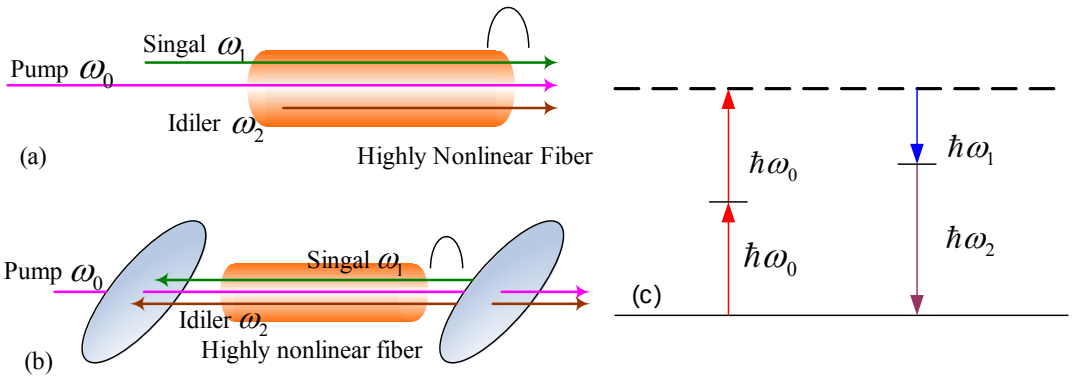

Fig. 3 (a) a single-pass parametric amplifier where a pump and signal are input to the system, and (b) a parametric oscillator where only a pump is input, but cavity feedback results in coherent buildup of a signal. (c) Annihilation of two "pump" photons and creation of two photons with different frequency.

Our current setup of FOPO is based on a piece of 4 cm PCF. In Fig. 4 the fiber has been placed within a Fabry-Perot cavity. By obtaining good cleaved ends of the fiber, using a properly chosen aspheric lens in front of the PCF, and choosing appropriate pump mode-matching lenses outside of the cavity, one can obtain low loss coupling through the short fiber. In practice, the value that one can obtain depends on the core size of the PCF that is being used, but 40% to 50% is typical for small core fibers (less than 2 um core diameter) and greater than 60% is typical for larger core fibers (greater than 4 um core diameter). The pump beam waist should be located near the input short-pass dielectric mirror (SPD) because that is also a location of the waist of the oscillating mode. Most PCFs exhibit some amount of birefringence, so the pump polarization should be aligned with the polarization modes of the fiber.

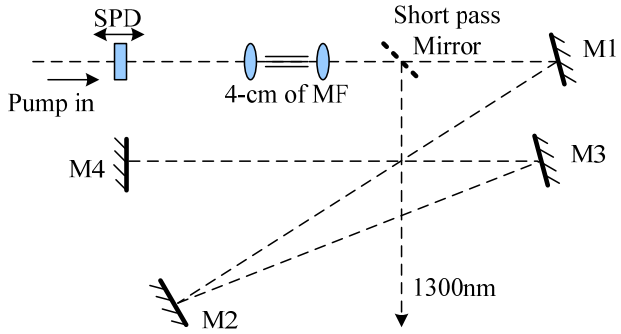

Fig. 4 A typical fiber-based OPO that utilizes a short PCF within a Fabry-Perot cavity. Pump coupling into the cavity is accomplished by using a short pass dielectric mirror (SPD). Aspheric lenses (AL) focus the beam into the microstructure

fiber, and the cavity is folded using broadband metallic mirrors M1-M3. Long wavelengths are reflected by both SPDs and thus oscillate within the cavity.

Parametric amplification is an ultrafast process mediated by the electronic susceptibility of the material. There is no long-lived excited state, so the FOPO cavity must be aligned so that it is synchronous with that of the pump laser cavity. The goal is to amplify the parametric scattering after each round trip through the system, and so a new pump pulse must be passing through the PCF when the photons generated by the previous pulse are passing through. Additionally, the ultrafast pump pulses can experience distortion upon propagation through the PCF. When the cavity is perfectly aligned then the system produces a stable pulse train with a minimum of amplitude fluctuations. Unstable amplitude fluctuations are present if the cavity is not perfectly synchronous.

It is critical to choose a fiber with the correct GVD behavior to obtain wideband parametric amplification [17]. One wants to choose a fiber and pump wavelength so that the system operates in the transition region between anomalous and normal GVD. The system will still operate over a fairly wide bandwidth when the pump laser is tuned slightly into the anomalous GVD, and in practice the system is much easier to align under these conditions. Oscillation is considerably more challenging to obtain for operation even slightly into the region of normal GVD.

The cavity lifetime is also an interesting consideration. The systems described previously have relatively lossless cavity mirrors at the oscillating wavelength, but suffer significant loss due to fiber input coupling. It is reasonable to estimate that the round-trip loss exceeds 70%. In order to identify the optimum oscillating signal feeback condition we must consider the goal of shifting as much energy as possible from the pump into the output conjugate field. Using this system we can independently adjust the feedback of the oscillating signal to obtain the optimum pump depletion.

The system depicted in Fig. 4 will operate at a center wavelength corresponding to the peak of the parametric gain. Wavelength tunability can be introduced by including a dispersive element within the cavity. If sufficient dispersion is added then the optical path length depends on wavelength. As such, the wavelength at which synchronous operation is achieved depends on the position of one of the end mirrors within the cavity.

We will show detailed experimental results of pulsed output based on phase retrieval of FROG measurement in the section 3.2

2.2 Self-similar pulse evolution in fiber optical parametric amplifiers and oscillators.

Since the FOPA is a central part of the FOPO, we will focus our theoretical study on the former. It can be modeled as four-wave mixing process based on the $\chi^{(3)}$ or Kerr nonlinearity. As illustrated in Fig. 3 (a), in the case of strong pumping such that the pump remains nearly undepleted, i.e. keep pump power P_0 constant. Then the other two pulses, signal wave A_1 and idler wave A_2, will satisfy the following coupled nonlinear Schrödinger equations (NLSEs) [22]:

$$\frac{\partial A_1}{\partial z}+\beta_{11}\frac{\partial A_1}{\partial t}+\frac{i}{2}\beta_{21}\frac{\partial^2 A_1}{\partial t^2}+\frac{1}{2}\alpha_1 A_1 = i\gamma\left[\left|A_1\right|^2+2\left|A_2\right|^2+2P_0\right]A_1+i\gamma P_0 A_2^* e^{-i\theta} \qquad (2)$$

$$\frac{\partial A_2}{\partial z}+\beta_{12}\frac{\partial A_1}{\partial t}+\frac{i}{2}\beta_{22}\frac{\partial^2 A_2}{\partial t^2}+\frac{1}{2}\alpha_2 A_2 = i\gamma\left[\left|A_2\right|^2+2\left|A_1\right|^2+2P_0\right]A_2+i\gamma P_0 A_1^* e^{-i\theta} \qquad (3)$$

where $\theta = (\Delta k + 2\gamma P_0)z$ is the phase matching parameter, β_{11} β_{12} are group velocities, β_{21} β_{22} are second order dispersions and α_1 α_2 are losses of each wave. Each NLSE Eq. (2) or Eq. (3) has dispersion term, self-phase modulation (SPM) term, cross-phase modulation (XPM) term and gain term. However, now in parametric amplifiers the gain is from the conjugation of other pulses through wave-mixing process. This is different from the model for Yb-doped fiber amplifiers or EDFA.

To gain some understanding of the dynamic pulse evolution of two pulses in the FOPA, we need to solve or simulate the coupled NLSEs Eq. (2) and (3). However, one can find that if two waves could have the relationship iA_2^* is proportional to A_1, the conjugated gain terms in Eq. (2) and (3) are related and the problem simplifies. This condition naturally arises when one of two fields A_1 or A_2 are taken to be zero at the input. Mathematically, we arrive at the same form of NLSE in Eq. (1) where Eq. (2) and (3) are independent and can be solved separately. This allows us to think about the easy situation, quasi CW, first. Since the pulsed FOPA usually works synchronously, this approximation is reasonable to simplify the model.

Suppose the length of the FOPA is l, and boundary conditions for the idler wave are $A_2(z=0)=0$ For CW situation, we omit second and third terms in the left of Eq. (2) , and the XPM term as comparing to the strong undepleted pump. When lossless, $\alpha_1 = 0$ and effective phase matched $\theta = (\Delta k + 2\gamma P_0)z = 0$ [10], the solution for the signal pulse propagation within, $0 < z < l$, is:

$$\begin{aligned} A_1(z) &= A_1(0)\cosh(\gamma P_0 z)\exp(-i\gamma 2P_0 z) \\ A_2(z) &= iA_1^*(0)\sinh(\gamma P_0 z)\exp(-i\gamma 2P_0 z) \end{aligned} \tag{4}$$

Therefore the generalized relation between two waves is:

$$iA_2^*(z) = A_1(z)\tanh(\gamma P_0 z)\exp(i\gamma 4P_0 z), \quad o < z < l \tag{5}$$

Then, for pulsed situation, we use this to replace the last term of the right side of Eq. (2) accompanied with transformations: $T = t - \beta_{11} z$, $B_1 = A_1\exp(-i\gamma 2P_0 z)$. Finally, we get:

$$\frac{\partial B_1}{\partial z} + \frac{i}{2}\beta_{21}\frac{\partial^2 B_1}{\partial T^2} = i\gamma(z)\left|B_1\right|^2 B_1 + \frac{g(z)-\alpha_1}{2}B_1 \tag{6}$$

where the gain coefficient is $g(z) = 2\gamma P_0 \tanh(\gamma P_0 z)$ and the nonlinearity is $\gamma(z) = \gamma[1 + 2\tanh^2(\gamma P_0 z)]$. Now Eq. (5) represents a single independent equation governing the propagation. Although the gain coefficient and nonlinearity are saturated rather than constants, the solutions for Eq. (6) still have asymptotic or self-similar behavior [25].

We simulate Eq. (6), and observe the self-similar behavior in Fig. 5. The scaling parameter, $\lambda = \max_t \left|B_1(z,t)\right|$, also leads to the rescaled amplitude $\left|\hat{B}_1(z,t)\right| = \lambda^{-1}\left|B_1(z,\lambda^{-1}t)\right|$..

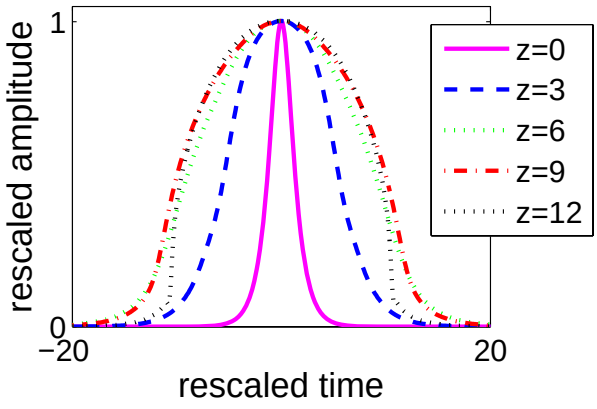

Fig. 5 The rescaled amplitude $\left|\hat{B}_1(z,t)\right|$ based on the simulation of normalized Eq. (5), where the rescaled time in each pulse is $\lambda^{-1}t$

Two characteristics can be indentified from Fig. 5: The pulse shape is more and more like parabolic shape during propagation. And after enough long distances, the pulse evolutes into a similariton or a self-similar pulse with asymptotic behavior. This result is consistent with pervious work [17-20], indicating that self-similar behavior is probably typical for generalized NLSE [25]. Our FOPA system has a high gain coefficient, and one can make the evolution distance short.

For example, using highly nonlinear fiber [24] for a FOPA set up , it is easy to obtain $\gamma P_0 > 100m^{-1}$ which makes the gain and nonlinearity in Eq. (6) saturate within a few millimeters. Therefore it is reasonable to rewrite gain coefficient and nonlinearity as constant- $g(z) = g = 2\gamma P_0$, $\gamma(z) = 3\gamma$. Then the asymptotic solution of Eq. (6) is [18]:

$$\Psi(z,T) = B_1(z,T)\exp\left(j\Phi(z,T)\right) \tag{6}$$

$$B_1(z,T) = B_0 \exp\left(\frac{g}{3}z\right)\sqrt{1-\frac{T^2}{T_p^2(z)}} \tag{7}$$

$$\Phi(z,T) = \varphi_0 + \frac{9\gamma B_0^2}{2g}\exp\left(\frac{2}{3}gz\right) - \frac{g}{6\beta_2}T^2, \tag{8}$$

where U_{in} is the initial pulse energy of signal pulse, $B_0 = \frac{1}{2}\left(\frac{gU_{in}}{\sqrt{3\gamma\beta_{21}/2}}\right)^{1/3}$ characterizes the amplitude of the pulse, $T_p = \frac{6\sqrt{3\gamma\beta_{21}/2}}{g}B_0\exp\left(\frac{g}{3}z\right)$ characterizes its width and φ_0 is an arbitrary constant.

Now one can easily indentify the scaling parameter is $\lambda = A_0\exp\left(\frac{g}{3}z\right)$. More precisely, the dimensionless product gz determines the rate at which parabolic pulses spread in time as well as at peak power. This tells us that a much higher gain will greatly cut down the evolution distance of similaritons.

In order to compare the performance of FOPA with former EDFA or Yb-doped fiber amplifier

methods [17,18], we suppose the gain coefficients, g, are $200m^{-1}$ and $2m^{-1}$ separately. Our comparison is based on a 10cm length FOPA and a 10m length usual fiber amplifier. One can find from the asymptotic solution Eqs. (6)- (8), g is in the denominator of the expression for Tp. This tells us that the large gain will not only cut down the evolution distance to reach self-similar propagation, but also efficiently make the pulse width shorter. Although the nonlinearity is in the numerator of the expression for Tp, the FOPA scheme only makes it three times bigger owing to XPM from the idler.

One can find the amplitude A_0 is proportional to $\left(g/\sqrt{\gamma}\right)^{1/3}$ and its width T_p is inversely proportional to $\left(g/\sqrt{\gamma}\right)^{2/3}$. Therefore, if the gain is a factor of 100 times larger, the output of peak power of the pulse will be 15 times higher while the pulse width will also be 15 times shorter. Thus, similar to gain-guided fiber scheme [20], this FOPA scheme will let the similariton generation have a much higher peak power output with shorter pulse duration. These features may have further applications in mode-locked normal dispersion fiber lasers [26] and similariton based optical communications [27].

3. CHARACTERIZATION OF SHORT PULSES: FREQUENCY RESOLVED OPTICAL GATING (FROG)

3.1 Principles of FROG

Full characterization of an optical pulse involves measurement of the complex envelope, i.e., the magnitude and phase of the wave function $U(t)=\sqrt{I(t)}\exp\left(j2\pi v_0 t+\varphi(t)\right)$, or equivalently the magnitude and phase of its Fourier transform $V(v)=\sqrt{S(v)}\exp\left(j\psi(v)\right)$. The spectrogram provides us this information.

The spectrogram of an optical pulse $U(t)$ is a time-frequency representation equal to the squared magnitude of the Fourier transform of the pulse as seen through a moving window or gating function $W(t)$:

$$S(v,\tau)=\left|\Phi(v,\tau)\right|^2;\quad \Phi(v,\tau)=\int U(t)W(t-\tau)\exp(-j2\pi vt)\,dt.$$

It can be measured by transmitting the pulse $U(t)$ through an optical gate controlled by a time-delayed gating function $W(t-\tau)$, and measuring the spectrum of the product $U(t)W(t-\tau)$ with a spectrum analyzer at each time delay τ, as depicted schematically in Fig. 6. An optical implementation relies on a moving mirror to introduce the time delay, an optical spectrum analyzer such as that shown in Fig. 7, and an appropriate optical gate. The technique is known as frequency-resolved optical gating (FROG) [28].

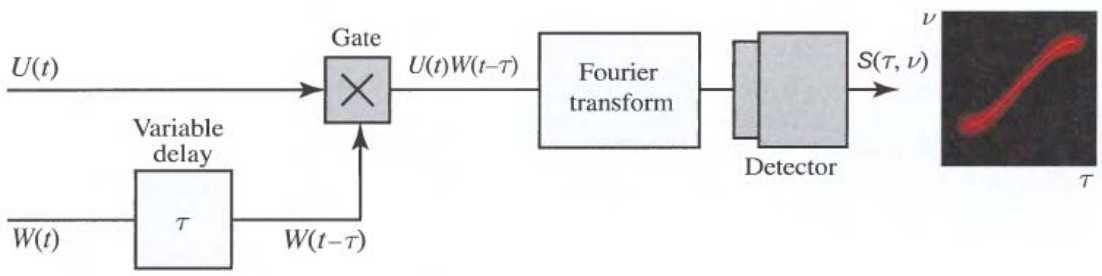

Fig. 6 Measurement of the spectrogram $S(v,\tau)$ by frequency-resolved optical gating (FROG) [38].

In the absence of a sufficiently short gating function $W(t)$, the pulse $U(t)$ itself, or another related pulse, may be used for this purpose. The relation between $W(t)$ and $U(t)$ depends on the nature of the used optical gate, as illustrated by the following examples:

For a second-harmonic generation (SHG) gate with input waves $U(t)$ and $U(t-\tau)$ at the fundamental frequency, the wave at the second-harmonic frequency is proportional to the product $U(t)U(t-\tau)$, so that $W(t) \propto U(t)$ and $\Phi(v,\tau) = \int U(t)U(t-\tau)\exp(-j2\pi vt)\,dt$.

This time-frequency function is known as the Wigner Distribution Function. The overall optical system that implements the block diagram in Fig. 6 is depicted in Fig. 7 and the system is known as the SHG-FROG. This system is suitable for single-shot measurement.

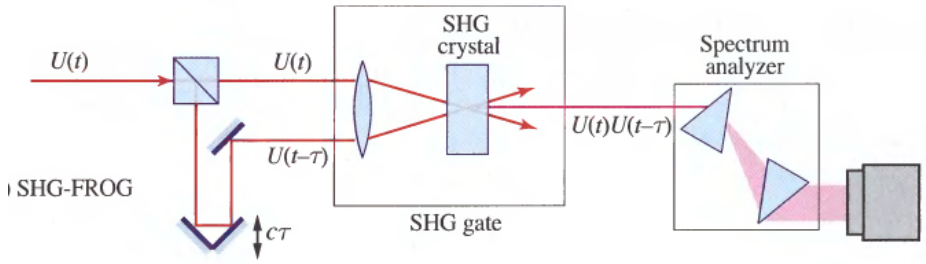

Fig. 7 The implementation of frequency-resolved optical gating (FROG): SHG-FROG [38].

However, experimentally, we usually need to do phase retrieval from the spectrogram we obtain. So the analysis is the opposite way. But then the initial phase of pulse is unknown. We need to guess this first and gradually change the phase. The problem of estimating $\Phi(v,\tau)$ from the measured $S(v,\tau) = |\Phi(v,\tau)|^2$ is a "missing-phase problem." One iterative approach follows the steps illustrated by the diagram:

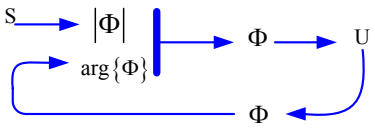

First, beginning with the measured spectrogram $S(\nu,\tau)$, the magnitude $\left|\Phi(\nu,\tau)\right| = \left\{S(\nu,\tau)\right\}^{1/2}$ is determined. Using some initial guess for the missing phase $\arg\left\{\Phi(\nu,\tau)\right\}$, the previous procedure [inverse Fourier transform $\Phi(\nu,\tau)$ with respect to ν and integrate over τ] is used to estimate $U(t)$ up to an unknown proportionality constant.

Then, knowing $U(t)$, $\Phi(\nu,\tau)$ is computed and a new estimate of the unknown phase $\arg\left\{\Phi(\nu,\tau)\right\}$ is determined and used in combination with the measured magnitude $\left|\Phi(\nu,\tau)\right|$ to obtain a new and better estimate of $U(t)$.

And the process is repeated until it converges to a pulse wave function $U(t)$ that is consistent with the measured spectrogram.

3.2 FROG Measurement results of FOPO

We built the SHG-FROG in our lab during last summer and fall semester and purchased pulse retrieval software from Femtosoft Technologies Ltd. We can use this powerful tool to characterize any short pulsed laser output- Ti: Sapphire, mode-locked fiber laser, or FOPO.

Two figures below are FROG screen shots showing the output from a FOPO based on the setup described in Fig. 4 in section 2.2. The wavelength can be “dispersion tuned” by adjusting the cavity length. Fig. 8 is the measurement of a perfectly synchronized cavity and Fig. 9 is the measurement of a slightly un-synchronized cavity.

In each figure, the top left panel is the measured spectrogram, where time delay is the horizontal axis and spectrum is in the vertical; the top middle panel shows the amplitude and phase of the retrieved electric field in time domain. The bottom middle panel is the spectral amplitude and spectral phase of the reconstructed field. The bottom left panel shows the reconstructed spectrogram. Two panels on the right side show the error based on this guess. The "Results" window in the near the bottom shows the parameters for the best fit (smallest error) of pulse.

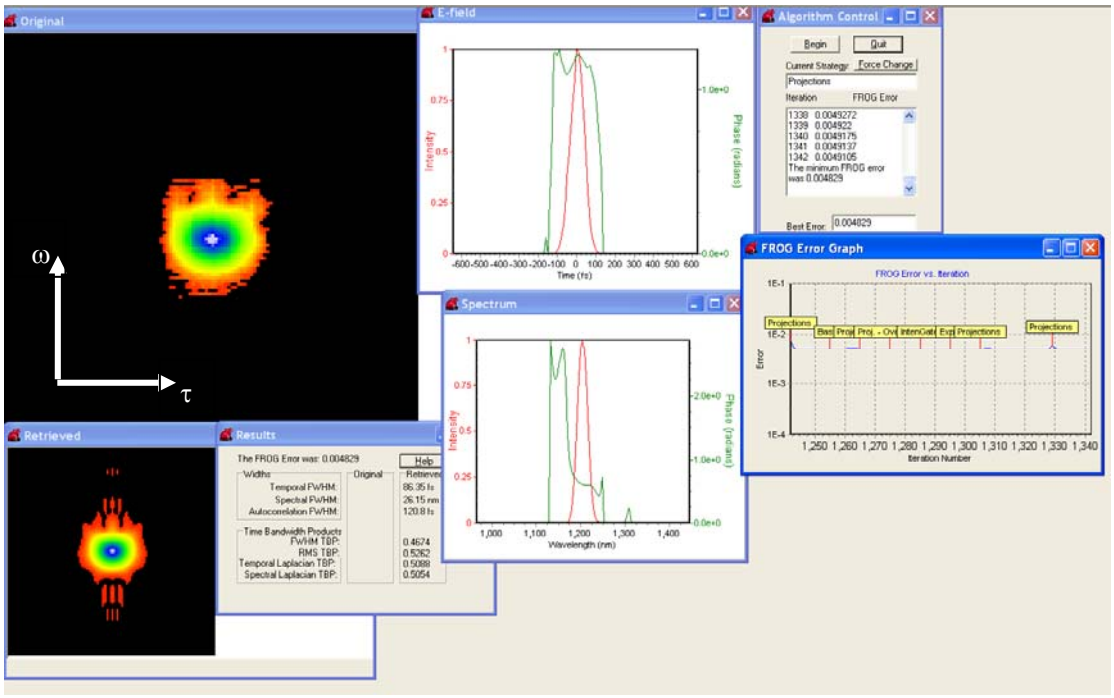

Fig. 8 Output pulse of Fiber OPO: Temporal FWHM: 86.35 fs, Center wavelength: 1212 nm

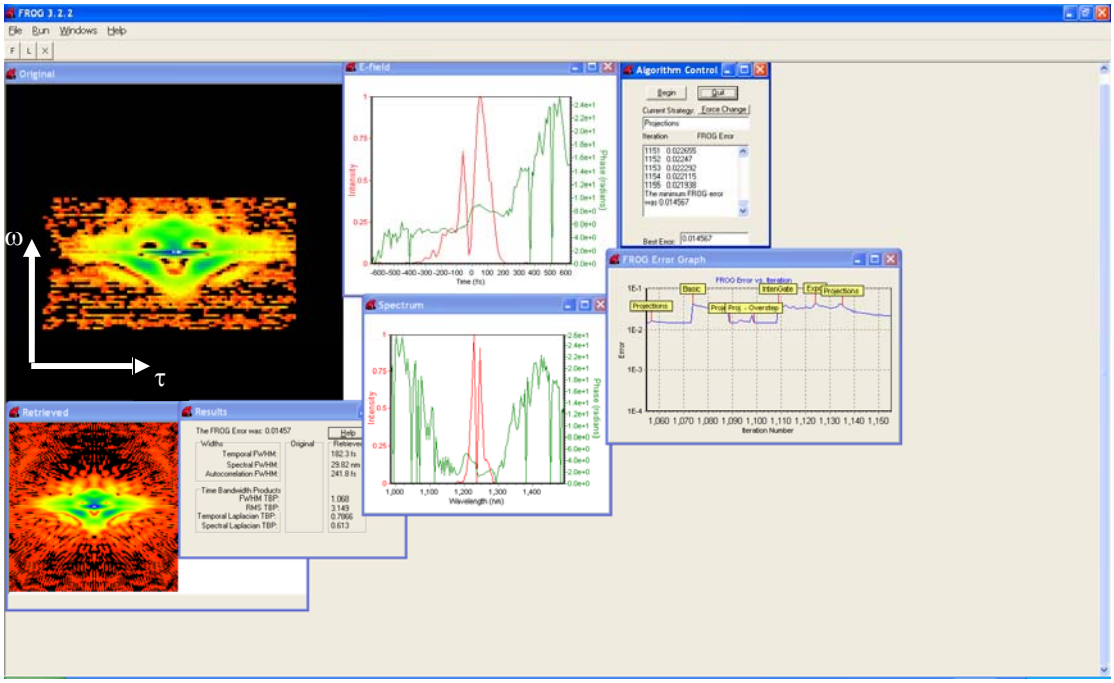

Fig. 9 Output pulse of Fiber OPO: Temporal FWHM: 182.3 fs, Center wavelength: 1262 nm

A comparison of the two figures clearly shows the change in pulse shape as the cavity length is changed. This is probably because the change of cavity length also changes the degree of synchronization leading to the asymmetric amplifier of signal pulses. And this asymmetric amplifier eventually makes the signal pulse having two peaks.

4. PROPOSED WORK

Much of the proposed work is geared towards understanding and improving the performance of FOPOs. Our preliminary FROG measurements show that the pulse shape of signal becomes complex as we vary the cavity length. There are at least two methods to solve this. Firstly one can attempt to separate the wavelength tunability from the cavity length, perhaps by using a tunable spectral filter. This will require a change to the design of the FOPO. Secondly, one can let the complicated pulse propagate within a FOPA such that it evolves into a similariton- parabolic pulse with linear chirp. The second approach is straightforward as we simply need another piece of PCF at the output of the FOPO.

4.1 Soliton and similariton propagation of the FOPO output

One of the advantages of the FOPO as a light source is the ability to tune the wavelength of the output into either the normal or anomalous dispersion ranges for commercially available PCFs. It is possible to obtain near-transform-limited pulses at the output of the FOPO for the perfectly synchronized cavity. These pulses can then be launched into an identical PCF configured as a parametric amplifier. Full characterization of the output as a function of power and amplifier length should display the expected self-similar pulse evolution. We can compare our simplified model for pulse propagation with experimental results to see how well it predicts behavior

The feasibility of this FOPA based similariton generation is studied in section 2.2. Figure 10 shows the experimental setup which we are currently working on. We use shorter wavelength pulse as signal output because 850 nm is in the normal dispersion for PCF (1300nm is anomalous dispersion for PCF.).

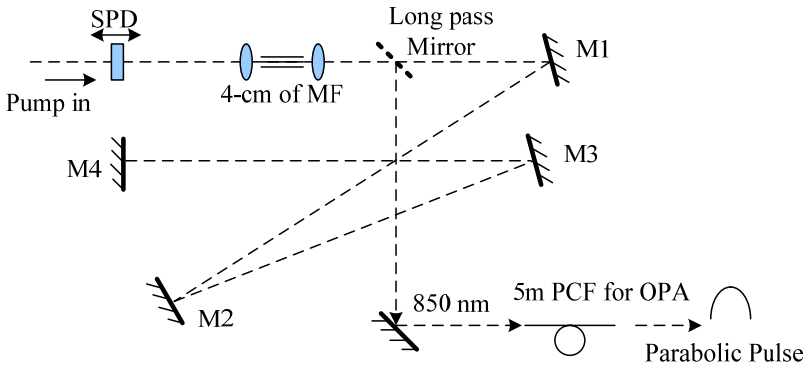

Fig. 10 Experimental setup for self-similar pulses evolution in FOPA

If the theoretical model developed is correct, our FROG measurement should show that both the input and output of FOFA is parabolic shape with quadratic phase (linear chirp). Furthermore, we can use the linear chirp to compress the pulse duration.

4.2 Improvement of pulse propagation model

As we made numerous assumptions, it will probably degrade the model for FOPA and FOPO. It will be better including pump depletion, dispersion, and a rapidly varying envelope in a coupled field

situation. And the biggest assumption is that we worked in an amplifier rather than an oscillator configuration. The model describing pulses within a cavity, including spectrally-dependent round trip losses and phase changes is no longer well described by the independent NLSE. It is important to explicitly include the time-dependent gain, which varies over the pulse envelope and the walk-off between the pump and signal pulses. A model which might be suitable for our situation is given as [34]:

$$\left[G(t) - L(t) + \delta T \frac{d}{dt} + \frac{1}{\omega_c^2} \frac{d^2}{dt^2} \right] \xi_1(t) = 0 \tag{9}$$

Eq. (9) describes the intensity profile of the repetitive signal pulses in the steady state. G(t) and L(t) are, respectively, the total round-trip electric field gain and loss. The cavity-detuning time, or walk-off between pulses, $\delta T = T - T_R$, is defined as the difference between the repetition time period of the pump pulses, T, and the round-trip propagation time, T_R, of the signal pulses. The cavity bandwidth, ω_c, is determined by the frequency-selective elements in the cavity.

The use of this model might be able to predict the complex pulse envelopes observed in our preliminary data and will give us a tool to use in making design choices to obtain output optimized for power, short pulses, or narrow spectrum.

4.3 Improvement and application of FOPOs

Armed with an improved understanding from the projects outlined above, we can consider new FOPO designs. First we will simply modify the accessible parameters in the existing configuration. We can optimize for power and short pulses by varying the amount of signal feedback, fiber length and dispersive properties of the optics currently being used. We can then modify the cavity so that the spectral tuning is independent on the cavity length. This way we can obtain "uncomplicated pulses" regardless of wavelength.

One application of FOPOs is to do optical manipulation. Our plan is use diffraction gratings to separate beams according to the wavelength, lens to focus each beam, a groove to serve as the room for manipulation in one dimension. So the goal is to use our FOPO as a tunable light source combining other optical components available in the lab, we can trap particles in one dimension. A similar idea based on Arrayed Waveguide Gratings was demonstrated by NTT in 2005 [39].

4.4 Other opportunities

Our primary goal is to optimize the performance of FOPOs for subsequent applications. There are, however, numerous problems of fundamental interest that involve pulse propagation in optical fibers.

- Improvement of pulse propagation tools [10, 11, 34].
- Observation of rogue waves in optical fibers [35, 36]
- Gain guided optical fibers & Novel designs of PCF [20, 29- 33]
- PCF based light source for CARS [37]

REFERENCE:

[1] P. St. J. Russell, "Photonic crystal fibers", Science 299, 358 (2003)

[2] W. J. Wadsworth, R.M. Percival, G. Bouwmans, J.C. Knight, T.A. Birks, T.D. Hedley, and P. St. J. Russell, "Very high numerical aperture fibers", IEEE Photon. Technol. Lett. 16, 843 (2004)

[3] T.A. Birks, J.C. Knight, and P.St.J. Russell, "Endlessly single-mode photonic crystal fibre", Opt. Lett. 22, 961 (1997)

[4] J. C. Knight, T. A. Birks; R. F. Cregan; P. St. J. Russell, and P. D. de Sandro, "Large mode area photonic crystal fibre", Electron. Lett. 34, 1347 (1998)

[5] A. Nolan, G. E. Berkey, M. Li, X. Chen, W. A. Wood, and L. A. Zenteno, "Single-polarization fiber with a high extinction ratio", Opt. Lett. 2, 1855 (2004)

[6] T. Schreiber, F. Röser, O. Schmidt, J. Limpert, R. Iliew, F. Lederer, A. Petersson, C. Jacobsen, K. Hansen, J. Broeng, and A. Tünnermann, "Stress-induced single-polarization single-transverse mode photonic crystal fiber with low nonlinearity", Opt. Express 13, 7621 (2005)

[7] L.A. Zenteno, J. Wang , D. T. Walton , B.A. Ruffin, M. J. Li, S. Gray, A. Crowley and X. Chen, "Suppression of Raman gain in single-transverse-mode dual-hole-assisted fiber", Opt. Express 13, 8921 (2005)

[8] J. C. Knight, J. Arriaga, T. A. Birks, A. Ortigosa-Blanch, W. J. Wadsworth, and P. St. J. Russell, "Anomalous dispersion in photonic crystal fiber", IEEE Photon. Technol. Lett. 12, 807 (2000)

[9] J. M. Dudley, "Supercontinuum generation in photonic crystal fiber", Rev. Mod. Phys. 78, 1135 (2006)

[10] G. P. Agrawal, "Nonlinear Fiber Optics" 4th edn, Academic, Boston, (2007).

[11] J. M. Dudley, C. Finot, D. J. Richardson, and G. Millot, "Self-similarity in ultrafast nonlinear optics", Nature Physics, **3**, 597-603 (2007).

[12] M. H. Dunn and M. Ebrahimzadeh, "Parametric generation of tunable light from continuous-wave to femtosecond pulses," Science 286, 1513-1517, Nov. 19, (1999).

[13] J. C. Diels, and W. Rudolph, Ultrashort laser pulse phenomena. San Diego: Academic Press, (1996).

[14] M. Dantus, and V. Lozovoy, "Experimental coherent laser control of physicochemical processes," Chem. Rev. 104, 1813-1859, (2004).

[15] F. Ganikhanov, S. Carrasco, X. Sunney Xie, M. Katz, W. Seitz, and D. Kopf, "Broadly tunable dual-wavelength light source for coherent anti-Stokes Raman scattering microscopy," Opt. Lett. 31, 1292-1294, (2006).

[16] V. G. Dmitriev, G. G. Gurzadyan, and D. N. Nikogosyan, "Optical parametric oscillation," in Handbook of nonlinear optical crystals. 3rd Ed. 345-362, New York: Springer, (1999).

[17] M. E. Fermann, V. I. Kruglov, B. C. Thomsen, J. M. Dudley, and J. D. Harvey, Phys. Rev. Lett.

84, 6010 (2000).

[18] J. M. Dudley, C. Finot, D. Richardson and G. Millot, Nature Physics, 3, 597 (2007).

[19] C. Finot, S. Pitois, G. Millot, C. Billet and J. M. Dudley, IEEE J. Sel. Top. Quant. Electron. 10, 1211–1218 (2004).

[20] C. Gu, B. Ilan, J. E. Sharping, “Parabolic Pulse Generation in Gain-Guided Optical Fibers with Nonlinearity”, ThZ 2, The 21st Annual Meeting of The IEEE Lasers & Electro-Optics Society (2008).

[21] M. Marhic, Fiber Optical Parametric Amplifiers, Oscillators and Related Devices. New York: Cambridge Univ. Press, (2007).

[22] G. P. Agrawal, Nonlinear Fiber Optics, 4th ed., Academic Press, New York, (2006).

[23] J. E. Sharping, J. R. Sanborn, M. A. Foster, D. Broaddus, and A. L. Gaeta, "Generation of sub-100-fs pulses from a microstructure-fiber-based optical parametric oscillator," Optics Express, 16, 18050 (2008).

[24] J. E. Sharping, "Microstructure Fiber Based Optical Parametric Oscillators," Journal of Lightwave Technology, 26, 2184 (2008).

[25] V. I. Kruglov, A. C. Peacock and J. D. Harvey, Phys. Rev. Lett. 90, 113902 (2003). V. I. Kruglov, and J. D. Harvey, J. Opt. Soc. Am. B 23, 2541 (2006).

[26] K. Kieu and F. W. Wise, "All-fiber normal-dispersion femtosecond laser," Optics Express 16, 11453 (2008).

[27] T. Hirooka, M. Nakazawa, and K. Okamoto, "Bright and dark 40 GHz parabolic pulse generation using a picosecond optical pulse train and an arrayed waveguide grating," Opt. Lett. 33, 1102 (2008).

[28] Rick Trebino, Frequency-Resolved Optical Gating: The Measurement of Ultrashort Laser Pulses. Springer (2002).

[29] A. E. Siegman, "Propagating modes in gain-guided optical fibers," J. Opt. Soc. Am. A. 20, 1617-1628 (2003).

[30] A. E. Siegman, "Gain-guided, index-antiguided fiber lasers," J. Opt. Soc. Am. A 24, 1677-1682 (2007).

[31] Y. Chen, T. McComb, V. Sudesh, M. Richardson, M. Bass, "Very large-core, single-mode, gain-guided, index-antiguided fiber lasers," Opt. Lett. 32, 2505 (2007).

[32] A. E. Siegmana, Y. Chen, V. Sudesh, M. Richardson, and M. Bass, P. Foy, W. Hawkins, and J. Ballato, “Confined propagation and near single mode laser oscillation in a gain guided, index antiguided optical fiber,” Appl. Phys. Lett. 89, 251101 (2006).

[33] T. Her "Gain-guiding in transverse grating waveguides for large modal area laser amplifiers," Optics Express, 16, 7197-7202 (2008)

[34] E. C. Cheung and J. M. Liu, "Theory of a synchronously pumped optical parametric oscillator in

steady-state operation," J. Opt. Soc. Am. B 7, 1385 (1990)

[35] D. R. Solli, C. Ropers, P. Koonath, and B. Jalali, “Optical rogue waves,” Nature 450, 1054-1058 (2007).

[36] D. R. Solli, C. Ropers, and B. Jalali, "Active control of optical rogue waves for stimulated supercontinuum generation," Phys. Rev. Lett. 101, 233902 (2008)

[37] A. A. Ivanov, A. A. Podshivalov, and A. M. Zheltikov, "Frequency-shifted megawatt soliton output of a hollow photonic-crystal fiber for time-resolved coherent anti-Stokes Raman scattering microspectroscopy, " Optics Letters, Vol. 31, 3318-3320.

[38] B. Saleh, M. Teich, Fundamentals of Photonics, Wiley, New York, (2007)

[39] T. Saida, T. Shibata, M. Ishii, and H. Takahashi, "Integrated Optical Tweezers Using Arrayed Waveguide Grating," CMEE6, Conference on Lasers and Electro-Optics (2005).

Appendix 4: CLEO 2012 submission of Chenji Gu

Spectral Mirror Imaging in Ultrafast Optical Parametric Processes

Chenji Gu*, Boaz Ilan and Jay E. Sharping

School of Natural Sciences, University of California - Merced, Merced, CA, USA, 95343

cgu2@ucmerced.edu

Abstract: We experimentally demonstrate and theoretically explore a spectral imaging system where two spectral sidebands produced through an optical parametric process always have reversed spectral profiles with respect to the center frequency of the pump.

OCIS codes: 060.2320, 060.4370, 060.5295.

Recently, advanced temporal imaging systems using optical fibers and silicon waveguides have been used to perform all-optical ultrafast waveform characterization tasks [1–5]. The principal idea in these experiments is the time lens [6], which imparts a quadratic phase modulation onto the input signal pulse. Linear dispersive pulse propagation, when combined with the time lens, completes a temporal imaging system which can generate, for example, an output idler with temporally reversed pulse shape compared with input signal [3]. Here we report a generalization of temporal imaging to the frequency domain. We demonstrate a spectral imaging system in which two spectral sidebands produced through an optical parametric process always have reversed spectral profiles. We call this phenomena spectral mirror imaging (SMI), and point out the fact that SMI is a spectral realization of temporal phase conjugation (TPC). Our experimental results reveal SMI features in the picosecond domain using a fiber optical parametric oscillator.

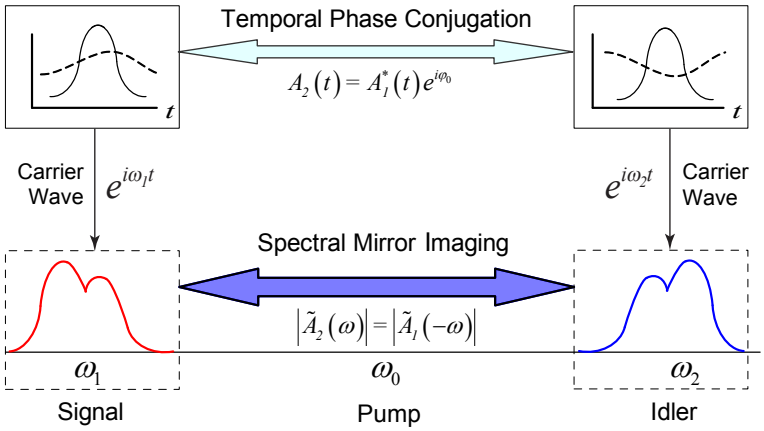

Fig. 1. Illustration of TPC in the time domain and SMI in the frequency domain.

One can define the complex wavefunctions of two optical pulses in the form $E_{1,2}(t) = A_{1,2}(t) \cdot e^{-i\omega_{1,2}t}$, where $A_{1,2}(t)$ are the complex envelopes independent from the rapidly varying carrier waves $e^{-i\omega_{1,2}t}$. The two pluses are characterized by the temporal amplitude $|A_{1,2}(t)|$ and the temporal phase $\arg\{A_{1,2}(t)\}$. In the frequency domain, the spectra of two pulses are described by Fourier transform $\mathscr{F}[E_{1,2}(t)] = \int_{-\infty}^{\infty} E_{1,2}(t) \cdot e^{-i\omega t} dt = \tilde{E}_{1,2}(\omega)$. Here $|\tilde{E}_{1,2}(\omega)|$ represent the spectral amplitudes. Since $\mathscr{F}[A_{1,2}(t)] = \tilde{A}_{1,2}(\omega) = \tilde{E}_{1,2}(\omega + \omega_{1,2})$ we see that the Fourier transforms of the complex envelopes $A_{1,2}(t)$ represent spectra of the same shape, but centered about different frequencies. Using this notation, SMI literally implies that two spectra shapes are spectrally inverted with respect to one another according to:

$$|\tilde{A}_2(\omega)| = |\tilde{A}_1(-\omega)|. \tag{1}$$

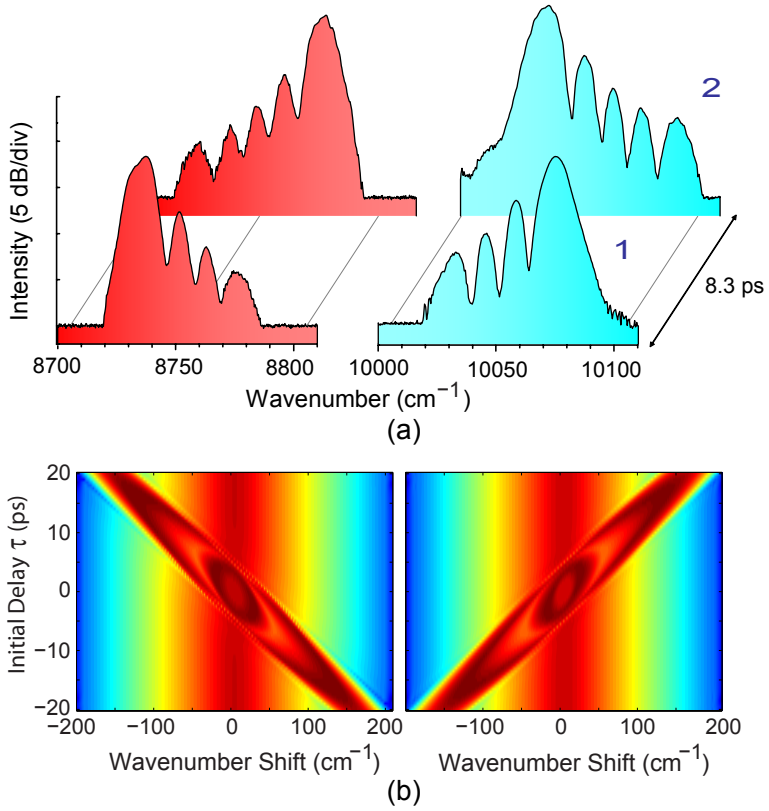

Fig. 2. SMI in the picosecond domain. (a) Measurement of the spectrum from the output of a system pumped by the picosecond laser. (b) Simulations of two sideband spectrograms.

In the optical frequency regime (visible to near IR) SMI happens naturally through pulsed optical parametric processes; and the mean of the center frequency of two sideband spectra, $(\omega_1+\omega_2)/2$, equals to the center frequency of pump ω_0 due to the photon energy conservation, i.e. $2\omega_0=\omega_1+\omega_2$.

Analogously, in the time domain, TPC implies that the phase profiles of two waves are reversed:

$$A_2(t)=A_1^*(t)\cdot e^{i\varphi_0}. \tag{2}$$

This relation indicates $\arg\{A_2(t)\}=\varphi_0-\arg\{A_1(t)\}$. The relationship between SMI and TPC follows from the Fourier transform of the complex envelopes of two pulses:

$$\tilde{A}_2(\omega)=\mathscr{F}[A_2(t)]=\mathscr{F}[A_1^*(t)\cdot e^{i\varphi_0}]=\tilde{A}_1^*(-\omega)e^{i\varphi_0}. \tag{3}$$

Notably, **SMI is a spectral realization of TPC** as shown in Fig. 1.

Figure 2 (a) shows our experimental observations of SMI between signal and idler in a picosecond-pumped fiber optical parametric oscillator. The shape of the output spectra depends on the cavity synchronization, which is adjusted by the end mirror [10]. In Fig. 2 (b) we present simulations of two sideband spectra. The pump pulse is an unchirped Gauss shape with the pulse duration of 8ps and the peak power at 780W. The input signal pulse is chosen to match the experimental conditions and is a chirped $sech^2$ shape with the pulse duration of 2ps and peak power of 5W.

The key finding is that spectral mirror imaging and temporal phase conjugation are connected at a fundamental level in many situations. In these situations, SMI is a spectral realization of temporal phase conjugation. We have explored this fundamental connection experimentally, theoretically, and numerically for ultra-fast $\chi^{(3)}$ nonlinear-optical parametric processes. The importance of this fundamental connection arises from the many applications of $\chi^{(3)}$ nonlinear-optical parametric processes. For example, techniques such as optical regeneration of temporal signals in communication systems [12], and turbidity suppression and imaging distortion correction of spatial signals can be achieved using $\chi^{(3)}$ processes. Promising multi-photon, label-free imaging techniques such as coherent anti-Stokes

Raman spectroscopic imaging will involve SMI-related signals. Ultrashort pulse characterization techniques rely on a firm understanding of the spectral and temporal characteristics of $\chi^{(3)}$ processes.

References

1. M. T. Kauffman, W. C. Banyai, A. A. Godil, and D. M. Bloom, "Time-to-frequency converter for measuring picosecond optical pulses", Appl. Phys. Lett. 64(3), 270-272 (1994).
2. M. A. Foster, R. Salem, D. F. Geraghty, A. C. Turner-Foster, M. Lipson, and A. L. Gaeta, "Silicon-chip-based ultrafast optical oscilloscope", Nature 456(7218), 81-84 (2008).
3. R. Salem, M. A. Foster, A. C. Turner, D. F. Geraghty, M. Lipson, and A. L. Gaeta, "Optical time lens based on four-wave mixing on a silicon chip", Opt. Lett. 33(10), 1047-1049 (2008).
4. R. Salem, M. A. Foster, A. C. Turner-Foster, D. F. Geraghty, M. Lipson, and A. L. Gaeta, "High-speed optical sampling using a silicon-chip temporal magnifier", Opt. Express 17(6), 4324-4329 (2009).
5. M. A. Foster, R. Salem, Y. Okawachi, A. C. Turner-Foster, M. Lipson, and A. L. Gaeta,"Ultrafast waveform compression using a time-domain telescope", Nat. Photonics 3(10), 581-585 (2009).
6. B. H. Kolner, "Space-time duality and the theory of temporal imaging", IEEE J. Quantum Electron. 30(8), 1951-1963 (1994).
7. M. E. Marhic, *Fiber optical parametric amplifiers, oscillators and related devices*, Cambridge Univ. Press, (2008).
8. G. P. Agrawal, *Nonlinear Fiber Optics*, 4th ed., Academic Press, New York, (2006).
9. C. Gu, B. Ilan, and J. E. Sharping, *To be published*.
10. C. Gu, C. Goulart, and J. E. Sharping, "Cross-phase-modulation-induced spectral effects in high-efficiency picosecond fiber optical parametric oscillators", Opt. Lett. **36**, 8, 1488-1490 (2011).
11. P. L. Baldeck, R. R. Alfano, and G. P. Agrawal, "Induced - frequency shift of copropagating ultrafast optical pulses", Appl. Phys. Lett. 52, 1939 (1988).
12. M. Gao, J. Kurumida, and S. Namiki, "Wavelength-tunable optical parametric regenerator", Opt. Lett. **35**, 20, 3468-3470 (2010).